Design and Performance of Visible Light Communication Systems

G V S S Praneeth Varma

A Thesis Submitted to
Indian Institute of Technology Hyderabad
In Partial Fulfillment of the Requirements for
The Degree of Doctor of Philosophy

भारतीय प्रौद्योगिकी संस्थान हैदराबाद
Indian Institute of Technology Hyderabad

Department of Electrical Engineering

Jan 2018

Declaration

I declare that this written submission represents my ideas in my own words, and where ideas or words of others have been included, I have adequately cited and referenced the original sources. I also declare that I have adhered to all principles of academic honesty and integrity and have not misrepresented or fabricated or falsified any idea/data/fact/source in my submission. I understand that any violation of the above will be a cause for disciplinary action by the Institute and can also evoke penal action from the sources that have thus not been properly cited, or from whom proper permission has not been taken when needed.
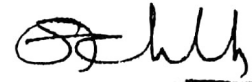
G. Praneeth Varma

(Signature)

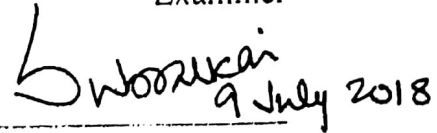(G V S S Praneeth Varma)

EE14 RESCH 11007

(Roll No.)

Approval Sheet

This Thesis entitled **Design and Performance of Visible Light Communication Systems** by G V S S Praneeth Varma is approved for the degree of Doctor of Philosophy from IIT Hyderabad.
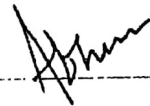
Prof. A. Chockalingam
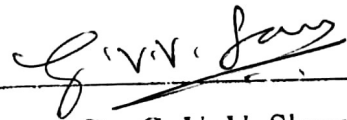
(IISC Bangalore)

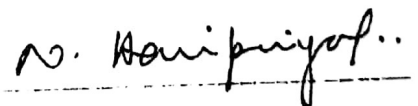Examiner

9 July 2018

Prof. Subrat Kar

(IIT Delhi)

Examiner

Dr. Abhinav Kumar

(IIT Hyderabad)

Internal Examiner

Dr. G. V. V. Sharma

(IIT Hyderabad)

Adviser

Dr. Haripriya Narasimhan

(IIT Hyderabad)

Chairman

Acknowledgments

This thesis would not be possible without the help and support of many people.

In particular, I would like to thank my advisor, Dr. G V V Sharma for his guidance and mentorship. His constant insights and ideas have helped me progress enormously in my research work. I am grateful for his support to investigate the broad areas that interest me and for having confidence in me. The frequent technical (and philosophical) discussions were intellectually very rewarding and helped me grow as a better person. I have thoroughly enjoyed my PhD studies and I attribute every bit of that happiness to Dr. Sharma.

I would like to thank my committee members, Dr. Abhinav Kumar, Dr. Vandana Sharma, Dr. Balasubramaniam Jayaram and Dr. Lakshmi Prasad Natarajan for their valuable suggestions which helped in completing my research in timely manner.

I am grateful to my hostel-mates, Sri Harsha, Sandeep Chandra, Naresh Reddy, Dr. Pankaj Kumar Jha, Dr. Kiran Kumar who are very close to me and made this journey very memorable.

I thank my lab colleagues, Hemanth Kumar, Tanmay Agarwal and others who assisted me in faculty development programs at various institutes.

I am forever indebted to my friends, Aditya Varma, Naveen Kumar, and Nagarjuna for motivating me and showing great faith in my abilities.

I also thank Anirudh for helping me with the documentation process.

I thank all my friends for their constant encouragement and unconditional support which made this journey enjoyable.

I would like to thank the faculty members and administrative staff at IIT Hyderabad for providing an ideal environment to pursue my dreams.

Dedication

To My Parents

for giving me the strength and support to pursue my dreams

Abstract

Light has traditionally been used for making objects visible to the naked eye. Lately, there has been tremendous interest in using it for free space communication. This has simultaneously been accompanied by significant interest in light emitting diodes (LEDs) that have been replacing conventional light sources in almost all applications like television, traffic lights, homes and offices etc. LEDs are better than existing incandescent lamps in terms of long life expectancy, high tolerance to humidity, low power consumption, and minimal heat generation. Fair amount of existing literature has focused on achieving uniform irradiance over a planar surface [1–7]. This has been addressed as the problem of finding the optimal LED geometry at the light source to achieve uniform irradiance. Several computationally intensive optimization routines like evolutionary, genetic algorithms were used for power allocation for the LED sources to realise uniform irradiance on the incident surface.

The most practical scenario would be the case when the LEDs are placed randomly at the source with uniform illumination being achieved through power allocation, keeping the total power constant. This is addressed as the first problem in this thesis by considering a binomial point process (BPP) based stochastic geometry. Further, a simple meta-heuristic power allocation scheme is proposed for uniform irradiance on the incident surface. Power allocation is done by maximizing a metric for uniformity of the signal to noise ratio (SNR) at the output of the photo-detector.

The performance of a stochastic visible light communication (VLC) system based on a BPP with a heuristic power allocation scheme to provide uniform irradiance is

analyzed in terms of bit error rate (BER). By intelligently using various approximations, an analytical expression for the BER for the BPP based VLC is obtained . This expression is then used to numerically obtain the optimum number of LEDs required for a stochastic VLC system. Such results for VLC are rare and usually restricted to light sources with a fixed geometry. The asymptotic BER for a circular BPP VLC is obtained in closed form and found to be numerically close to that for a square BPP. The BER expression is used to estimate the cost of the VLC system in terms of the number of LEDs required for optimum system performance.

While a BPP based stochastic model is a powerful tool for resource allocation for VLC, it is useful to consider power allocation for a VLC based on a single realization of a stochastic point process. Here, a Matern type II hard-core point process (HCPP) is desirable, since it accounts for minimum separation between any two LEDs for better coverage. This is the focus of the next problem addressed in the thesis. The variance of the power on the receiver plane is used as an objective function. Under some conditions, this function is shown to be convex, allowing for optimum power allocation. Through numerical results, it is shown that this approach is superior to existing techniques for power allocation.

Contents

List of Figures

List of Tables

Nomenclature

$_1F_2$ Gauss Hypergeometric function

$\bar{\Lambda}$ Mean of SNRs Λ_j on receiver plane

Λ_j SNR at j^{th} photo-detector

$\mathbb{E}[\cdot]$ The expectation operator

$\mathcal{B}$ Beta function

Φ Point Process

$\phi_{\frac{1}{2}}$ LED semi-angle at half power

var$[\cdot]$ Variance of a random variable

var$[\Lambda]$ Variance of SNRs Λ_j on receiver plane

$B(a,r)$ Ball of radius r centered at a

d_{ij} Distance between i^{th} LED and j^{th} photodetector

F_Λ Quality factor

h Distance between the transmit and receive surfaces

H_{ij} Propagation loss with distance

M_I Modulation Index

N Number of source LEDs

n_j AWGN at j^{th} photo-detector

P_e Probability of error

P_{r_j} Received power at j^{th} photo-detector

P_{t_i} Transmit power at i^{th} node

$Q(\cdot)$ Q-function

x_i Symbol transmitted by the ith LED

AWGN Additive White Gaussian Noise

BER   Bit Error Rate

BPP   Binomial Point Process

CDF   Cumulative Distribution Function

DD   Direct Detection

HCPP Hard-Core Point Process

IM   Intensity Modulation

LED   Light Emitting Diode

MIMO Multiple Input Multiple Output

OOK   On-Off Keying

PDF   Probability Density Function

PLA   Piecewise Linear Approximation

SNR   Signal to Noise Ratio

VLC   Visible Light Communication

Chapter 1

Introduction

Optical Wireless communication (OWC) is a general term which refers to all types of optical communications like VLC, free space optics (FSO), light fidelity (Li-Fi) and infra-red. VLC is a subset of optical wireless communications technologies. VLC uses visible light spectrum between 400 and 800 THz (780–375 nm) as a medium for communication.

A design of new communication technologies is crucial to overcome the drawbacks of the RF communication systems. VLC serves the purpose in overcoming them. VLC systems employ visible light for communication that utilize the spectrum from 375 nm to 780 nm resulting in bandwidth of 400 THz. This spectrum is non-licensed and approximately 10^4 times the radio frequency (RF) spectrum solving the problem of bandwidth limitation in RF. Unlike RF waves, the light cannot penetrate through walls and thus, it is immune to security issues that arises in the RF communication systems. The increase in RF power beyond a certain threshold would result in health issues to humans. A regulatory body is administered to standardize and control the RF power and spectrum. In VLC, the power used for illumination also serves the purpose of communication as well. A rise in optical power results in higher illumination and this can be seen by the eye which enables people to respond accordingly.

1.1   Related Work

There has been tremendous interest in using it for free space communication [8]. This has simultaneously been accompanied by significant interest in light emitting diodes (LEDs) that have been replacing conventional light sources in almost all applications [9–11]. LEDs are better than existing incandescent lamps in terms of long life expectancy, high tolerance to humidity, low power consumption, and minimal heat

generation. Fair amount of existing literature has focused on achieving uniform irradiance over a planar surface [1–3, 12], beginning with the problem of finding the optimal LED geometry at the light source to achieve uniform irradiance [4]. This was done by using the irradiance distributions at the closest points on the incident surface. The case of LEDs using a free-form lens with a large view angle has been considered in [13]. More literature on similar themes is available in [14, 15]. In [16], the properties of white LEDs were studied and shown to be useful for indoor optical transmission. More literature on using white LEDs for communication is available in [17–20].

Some of the above literature has focused on a regular geometry with equal power allocation to individual LED sources. While uniform illuminance is desirable, optimal power consumption is an extremely important factor in the design of LED light sources. To address this, recent literature has focused on power allocation, along with flexiblity in the LED source geometry to achieve uniform irradiance [5, 6, 21, 22].

Several power allocation schemes have been proposed to achieve uniform irradiance for visible light communication (VLC) applications [5,6,21,22]. A trial and error approach for power allocation for uniform irradiance is used in [21] for a combination of circular square geometry in order to illuminate the edges of the incident surface. An evolutionary algorithm based optimization scheme is proposed in [6] to modify the power of LED transmitters to reduce the signal power fluctuation at the receiver. In [5], a genetic algorithm is proposed to optimize the refractive indices of the concentrators on receivers to achieve a uniform distribution of the received power. An optimal LED arrangement to achieve uniform irradiance is investigated as a convex optimization problem in [22]. The optimization of the location of an irregular LED array for uniform irradiance is discussed in [7, 23].

1.2   Research Contributions of This Thesis

- A simple heuristic power allocation scheme is proposed for a random LED array to obtain uniform irradiance on the receiver plane. This is done by considering a binomial point process (BPP) for modeling the LED location and using the quality factor as a performance metric. Numerical results are provided to validate the proposed model and demonstrate its simplicity over existing LED geometries.

- Once it is established that BPP modeling can achieve uniform illuminance in an

average sense, we analyzed the BER performance of VLC for a BPP model. A theoretical closed form approximation for the asymptotic bit error rate (BER) is obtained and used for estimating the cost of the visible light communication (VLC) system in terms of the number of LEDs as well as the power required for satisfying the system performance requirements.

- There are some scenarios where LED sources in a VLC system cannot be placed at certain locations due to design restrictions. Such cases can be modeled by approximating the square BPP with multiple non-overlapping circles. This process is referred as circle-square BPP. We present the BER performance analysis of circle-square BPP and compare it with square BPP.

- While we have established the uniform illumination in the average sense, it would be interesting to find the optimum power allocation for a single realization of a random geometry. So an optimal power allocation scheme is proposed to achieve uniform illuminance. Regular arrays and random geometries are considered for an arrangement of the source LEDs. Uniform illuminance is accomplished by considering the variance of the received power on the receiver plane as a metric and framing it as a convex optimization problem. Numerical results show that the quality factor of random geometries are superior to fixed geometries. While preserving uniformity, the cost of the system can be reduced when random geometries are used.

1.3   Thesis Organization

The overall operation of a general LED based VLC system and relevant background information is discussed in chapter 2. In chapter 3, we present heuristic based power allocation scheme for a random LED array. Further analysis of BER performance for a VLC system using BPP model is discussed in chapter 4. Further BER performance analysis of circle-square BPP model is presented in chapter 5. We address the optimum power allocation for a single realization of a random geometry in chapter 6. The final conclusions and future research scope is discussed in chapter 7.

Chapter 2

System Model

2.1 Operation of Visible Light Communication System

Let us understand how the VLC system communicates with a simple example of transmitting data in form of digital signals '0's and '1's. An ordinary light is used to send the data. It is turned on when '1' is to be transmitted and turned off when '0' is to be transmitted. But when '0' is transmitted the light is turned off, it doesn't meet the purpose of illumination. Now if the light is switched on and off continuously at high rate, then the light appears to be constant. It serves the purpose of both illumination and communication at the same time. A human eye can perceive this flickering effect upto a frequency of 100 to 120 Hz. The fluorescent lamps or ordinary lamps can transmit signals at 10 Kbps and light-emitting diodes (LEDs) can reach upto 500 Mbps.

2.1.1 Propagation of Light from LED

Using the Lambertian radiation pattern to model the LED radiant intensity, [10, 11]

$$R_o\left(\phi\right) = \frac{\left(m+1\right)\cos^m\left(\phi\right)}{2\pi},\tag{2.1}$$

where ϕ is the angle of incidence of light on the surface and m is the order of Lambertian emission, with $\phi_{\frac{1}{2}}$ being the LED semi-angle at half power, provided by the manufacturer.

In Fig. 2.1, the transmitter emits an axially symmetric radiation pattern described by the radiant intensity $P_t R_o\left(\phi\right)$. A receiver located at a distance d at an angle ϕ with
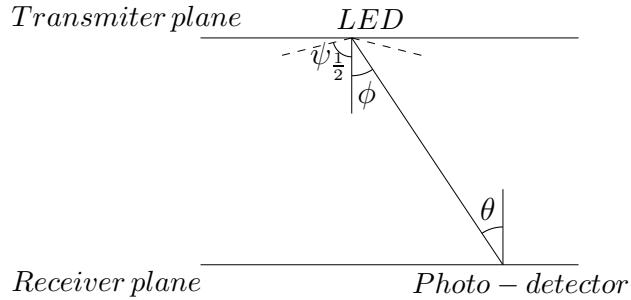
Figure 2.1: Propagation model

respect to (w.r.t.) transmitter the irradiance is $\frac{P_t R_o(\phi)}{d^2}$. Ignoring reflection losses, a detector achieves an effective signal-collection area of

$$A_{eff} = A\cos(\theta) \tag{2.2}$$

where A is the detector physical area and θ is the angle of incidence with respect to the receiver axis. The power received at the receiver is given by

$$P_r = \frac{P_t R_o(\phi) A_{eff}}{d^2} \tag{2.3}$$

The parameter that characterizes the channel is DC channel gain which can then be expressed as [10, 11]

$$H = \frac{R_o(\phi)\cos(\theta)A}{d^2} = \frac{(m+1)\cos^m(\phi)A\cos(\theta)}{2\pi d^2} \tag{2.4}$$

where d is the distance between the LED and the photo-detector, A is the physical area of photo-detector, and θ is the inclination of the photo-detector to the incident surface.

2.1.2 Transmitters

A huge opportunity for VLC is created because of the widespread use of LEDs. LEDs are semiconductor devices that can switch at very high speeds that was not possible with fluorescent and incandescent lamps. The low cost, lesser power consumption, longer lifetime, smaller size, and less heat dissipation are the additional features of LEDs. The LEDs are chosen as the transmitters or light sources in VLC because of the above listed advantages.
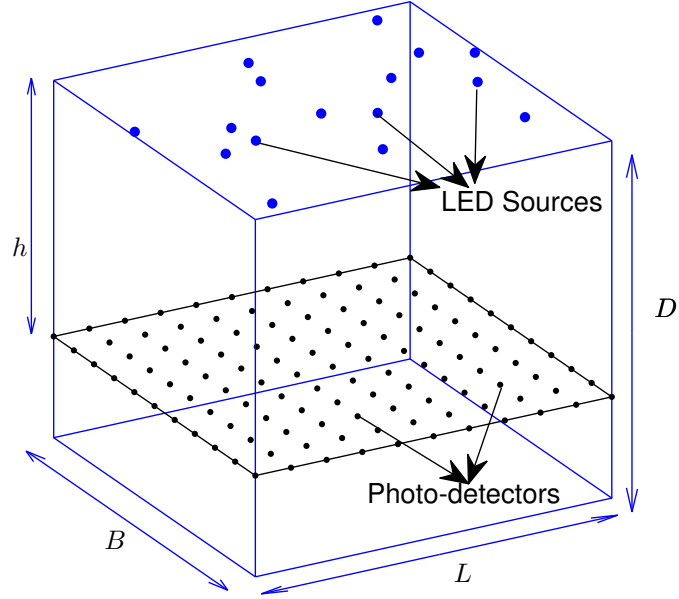
Figure 2.2: Realization of BPP with 16 LEDs

2.1.3 Receivers

In the typical VLC, the light is detected using a photo-diode and then converted into a electrical signal. In case of mobility, the image sensor can be used in place of a photo-diode because of its larger field-of-view (FOV). The drawback of image sensors are more power consuming and slow operating. Image sensors are available in all the handheld smart phone devices this drives towards adopting to VLC systems at no additional cost.

2.2 Trans-receiver Model

Consider the random source geometry generated using a BPP for $N = 16$ LEDs as shown in Fig. 2.2. The photo-detectors lie in a plane parallel to the LED array plane. The optical signal transmitted by the ith LED of the VLC in Fig. 5.1 is given by [21]

$$p_i(t) = P_{t_i} \left[1 + M_I x_i(t) \right], \tag{2.5}$$

Table 2.1: System Model Parameters.

Symbol	Description
$P = \sum_{i=1}^{N} P_{t_i}$	Total power allocated to the source
r_i	Distance of the ith LED from the centre of the square in Fig. 1
$H_{ij} = \frac{(m+1)A\cos^m(\phi)\cos(\psi)}{2\pi d_{ij}^2}$	Propagation loss with distance
$m = \frac{\ln\left(\frac{1}{2}\right)}{\ln\left(\cos\left(\phi_{\frac{1}{2}}\right)\right)},$	Order of Lambertian emission
R	Responsivity
$\phi = \cos^{-1}\frac{h}{d}$	Angle of incident light
ψ	Inclination of the photodetector to the incident surface

where, P_{t_i} is the transmit power at the ith LED, x_i is the corresponding modulating bipolar OOK signal and M_I is the modulating index [24]. Here the former term (P_{t_i}) in (2.5) takes care of illumination while the latter $(P_{t_i}M_I x_i)$ is for communication. After photo-detection, assuming that the DC component of the detected electrical signal is filtered out at the receiver, the received signal at photo-detector j is given by

$$y_j = RP_{r_j} + n_j \tag{2.6}$$

where

$$P_{r_j} = \sum_{i=1}^{N} H_{ij} P_{t_i} M_I x_i \tag{2.7}$$

All the above parameters are defined in Table 2.1. More details are available in [21,25]. The BPP in Fig. 2.3 represents the possible distribution of LEDs at the source. The square in all the figures in Fig. 2.3 has edge L. All the LEDs are located vertical to the plane where the photo-detector is placed.

2.2.1 Noise at the photo-detector

The noise at the photo-detector is the sum of the contributions from shot noise and thermal noise, and expressed as [26]

$$\sigma_j^2 = \sigma_{shot}^2 + \sigma_{thermal}^2, \tag{2.8}$$

Table 2.2: Sample noise parameters

Parameters	Symbol	Configuration
Boltzmann constant	k	$1.38064852 \times 10^{-23} m^2 kg s^{-2} K^{-1}$
Electronic charge	q	$1.60217662 \times 10^{-19} C$
Area of Photo-detector	A	$10^{-4} m^2$
Fixed capacitance of photo-detector	η	$112 pF/cm^2$
Responsivity	R	$1A/W$
Noise bandwidth	B_N	$100 MHz$
Background current	I_{bg}	$5100 \mu A$
Noise bandwidth factors	I_2, I_3	$0.562, 0.0868$
Absolute temperature	T_k	$295K$
Open-loop voltage gain	G	10
FET channel noise factor	Γ	1.5
FET trans-conductance	g_m	$30 mS$

where

$$\sigma^2_{shot} = 2qRP_{r_j}B_N + 2qI_{bg}I_2B_N,$$
$$\sigma^2_{thermal} = \frac{8\pi k T_k}{G}\eta A I_2 B_N^2 + \frac{16\pi^2 k T_k \Gamma}{g_m}\eta^2 A^2 I_3 B_N^3 \tag{2.9}$$

with the parameters defined in Table. 2.2.

2.2.2 Modulation technique

The modulation scheme employed for performance analysis is On-Off Keying (OOK). In VLC, the power to the LED transmitter is modulated to transmit '1's and '0's. Since the power is always non-negative, unlike conventional digital modulation techniques. The modulated signal is $P_t(1 + x_i)$, x_i assumes bipolar symbols +1 and -1 for bits '1' and '0' respectively. This power drives the source LEDs which results a change in intensity and hence the name intensity modulation (IM)

2.2.3 Detection technique

The receivers used for detection are photo-diodes. The photons emitted by light sources hits the photo-diode, electron-hole pairs are created in the depletion region of the photo-diode. This mechanism is called as the inner photoelectric effect. The

holes in the depletion region move towards the anode, and electrons move towards the cathode producing a photocurrent. Thus the photo-diode converts the optical energy into electrical signal. This is known as direct detection (DD). Note that if multiple sources transmit the signal, the signal at photo-detector is the sum of all the received signal from individual sources.

2.3 Point process

A point process is a collection of points randomly located on the space such as the real line, the Cartesian plane etc.. Point processes or stochastic processes is a powerful tool in statistics for modeling and analyzing spatial data. These point processes are frequently used as models for random events in time like location of base stations in a telecommunication network. Generally the point processes depends on some random measure. If the random measure follows a Poisson random variable, such a process is called Poisson point process (PPP). The average density of the points in the Poisson process located in some space is constant, then the resulting point process is called a homogeneous or stationary Poisson point process.

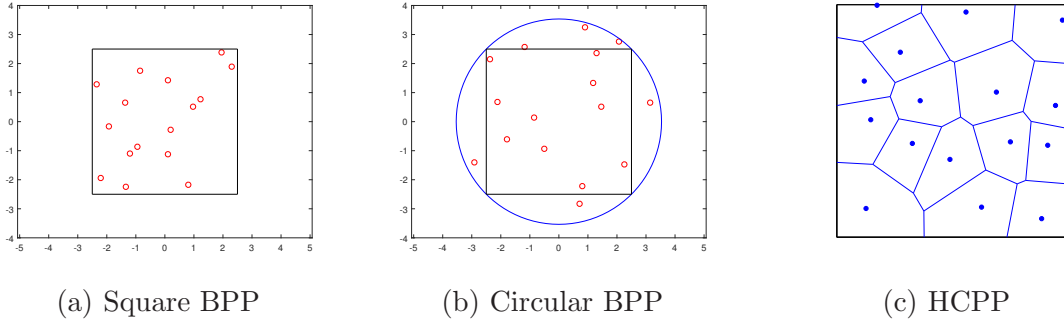(a) Square BPP (b) Circular BPP (c) HCPP

Figure 2.3: Arrangement of $N = 16$ LEDs for different geometries.

2.3.1 Square BPP

The square BPP in Fig. 3.1b provides a realistic distribution of light sources in an indoor environment, where N LEDs are placed randomly within a square of edge L at the points $(a_n, b_n) : a_n, b_n \sim U(-L/2, L/2), \forall n = \{1 \cdots N\}$, according to a uniform

distribution U defined by

$$f_U(u) = \begin{cases} \frac{1}{L} & -\frac{L}{2} \le u \le \frac{L}{2} \\ 0 & \text{otherwise} \end{cases} \tag{2.10}$$

2.3.2 Circular BPP

The circular BPP in Fig. 3.1d provides a reasonable approximation to the square BPP in Fig. 3.1b, where N LEDs are placed randomly within a circle of radius R_c at the points $(a_n = r_n \cos\theta_n, b_n = r_n \sin\theta_n) : \theta_n, r_n$, according to distributions $\Theta, \mathcal{R}$ defined by the probability density functions (PDF)

$$f_\Theta(\theta) = \begin{cases} \frac{1}{2\pi} & 0 \le \theta \le 2\pi \\ 0 & \text{otherwise} \end{cases} \tag{2.11}$$

$$f_\mathcal{R}(r) = \begin{cases} \frac{2r}{R_c^2} & 0 \le r \le R_c \\ 0 & \text{otherwise} \end{cases} \tag{2.12}$$

where Θ is a random variable distributed uniformly between $(0, 2\pi)$ and f_Θ is the corresponding probability density function (PDF) and $\mathcal{R}$ is a random variable distributed between $(0, R_c)$ and $f_\mathcal{R}$ is the corresponding PDF. Though the BPP process captures the uniform distribution of LEDs, each realization of the process may result in two LEDs at the same location leading to high interference. This can be avioded by ensuring a minimum separation between the LEDs. Matern is one such point process.

2.3.3 Matern process of type II

The HCPP in Fig. 2.3c resembles the possible distribution of LEDs at the source. In this point process, points are generated from a stationary parent Poisson point process (PPP) of intensity λ_{ppp} and a random mark is associated with each point, and a point of the parent Poisson process is deleted if there exists another point within the hard-core distance δ with a smaller mark. The intensity of the Matern point process is [27]

$$\lambda_{mpp} = \lambda_{ppp} e^{-\lambda_{ppp}\pi\delta^2} \tag{2.13}$$

10

2.4 Performance metric

The quality factor, defined in [21] for measuring the irradiance performance of the light source, can be expressed as

$$F_\Lambda = \frac{\overline{\Lambda}}{2\sqrt{\text{var}(\Lambda)}}, \tag{2.14}$$

where

$$\Lambda_j = \frac{P_{r_j}^2}{\sigma_j^2} \tag{2.15}$$

is the received signal to noise ratio (SNR) at the jth photo-detector and $\overline{\Lambda}$ and $\text{var}(\Lambda)$ are the mean and variance of $\{\Lambda_j\}_{j=1}^K$, where K is the number of photo-detectors. For uniform illumination, it is important that the mean $\overline{\Lambda}$ be large and the variance $\text{var}(\Lambda)$ be small, resulting in (2.14). Since the output of the photo-detector is an electrical signal which is affected by noise, it is important to consider the SNR Λ_j while computing the quality factor in (2.14).

11

Chapter 3

Power Allocation for Uniform Illumination with Stochastic LED Arrays

Recent research in LED based VLC system have focused on achieving uniform irradiance over a planar surface with the goal of finding the optimal LED geometry at the light source to achieve uniform irradiance [4]. This has been achieved by using irradiance distributions at the closest points on the incident surface. In some of the other research work [17–20], the properties of white LEDs were studied and shown to be useful for indoor optical transmission.

Also, fair amount of focus has gone on achieving uniform irradiance with a regular geometry with equal power allocation to individual LED sources [1–3, 12]. While uniform illuminance is desirable, optimal power consumption is an equally and sometimes more important factor in the design of LED light sources especially in modern IoT based applications. To address this, recent research has focused on power allocation, along with flexiblity in the LED source geometry to achieve uniform irradiance [5, 6, 21, 22].

To achieve this, several power allocation schemes have been proposed to achieve uniform irradiance for visible light communication (VLC) applications [5, 6, 21, 22]. For example a trial and error approach for power allocation for uniform irradiance is used in [21] for a combination of circular square geometry in order to illuminate the edges of the incident surface. An evolutionary algorithm based optimization scheme is proposed in [6] to modify the power of LED transmitters to reduce the signal power fluctuation at the receiver. In [5], a genetic algorithm is proposed to optimize the refractive indices of the concentrators on receivers to achieve a uniform distribution

of the received power. An optimal LED arrangement to achieve uniform irradiance is investigated as a convex optimization problem in [22]. The optimization of the location of an irregular LED array for uniform irradiance is discussed in [7, 23].

3.1 Cost-effective approach to achieve uniform illumination

In all the above approaches, computationally intensive optimization routines were used for power allocation for the LED sources to realise uniform irradiance on the incident surface. The system proposed in [22] departs from the conventional model by considering arbitrary locations for the LED sources. The most practical scenario would be the case when the LEDs are placed randomly at the source with uniform illumination being achieved through power allocation, keeping the total power constant.

This problem is addressed in this Chapter by considering a binomial point process (BPP) based stochastic geometry [28]. Further, a simple meta-heuristic power allocation scheme is proposed for uniform irradiance on the incident surface. Power allocation is done by maximizing a metric for uniformity of the signal to noise ratio (SNR) at the output of the photo-detector. Through numerical results, it is shown that the performance of the BPP model and the associated power allocation is comparable to the model in [21].

Consider the various source geometries for $N = 16$ LEDs in Fig. 3.1. Using (2.15), the respective SNR profiles for the sources in Fig. 3.1a and 3.1b are plotted in Fig. 3.2, when each of the LEDs has equal power. Circular geometries are limited by their inability to sufficiently illuminate the corners of the incident surface. Figure 3.3a has the SNR profile for the source in Fig. 3.1d, with optimal locations for the LEDs on the circle as well as the corners [21] with equal power. Due to this optimal location, the arrangement in Fig. 3.1d has a more uniform SNR profile, since the coverage at the edges is better. The performance improves with optimal power allocation, as shown in Fig. 3.3b.

Figure 3.3 and [21] indicate that LED sources distributed over an area according to a fixed geometry can achieve uniform irradiance with optimal location and power. In practice, LED sources used for illuminating larger areas may not follow a fixed geometry. When the locations of the LED sources are fixed but do not follow a definite pattern, like in Fig. 3.1c, the geometry can be modeled using a BPP. In

(a) Circular geometry

(b) Concentric circular geometry

(c) A realization of BPP

(d) Circle-square geometry in [21]
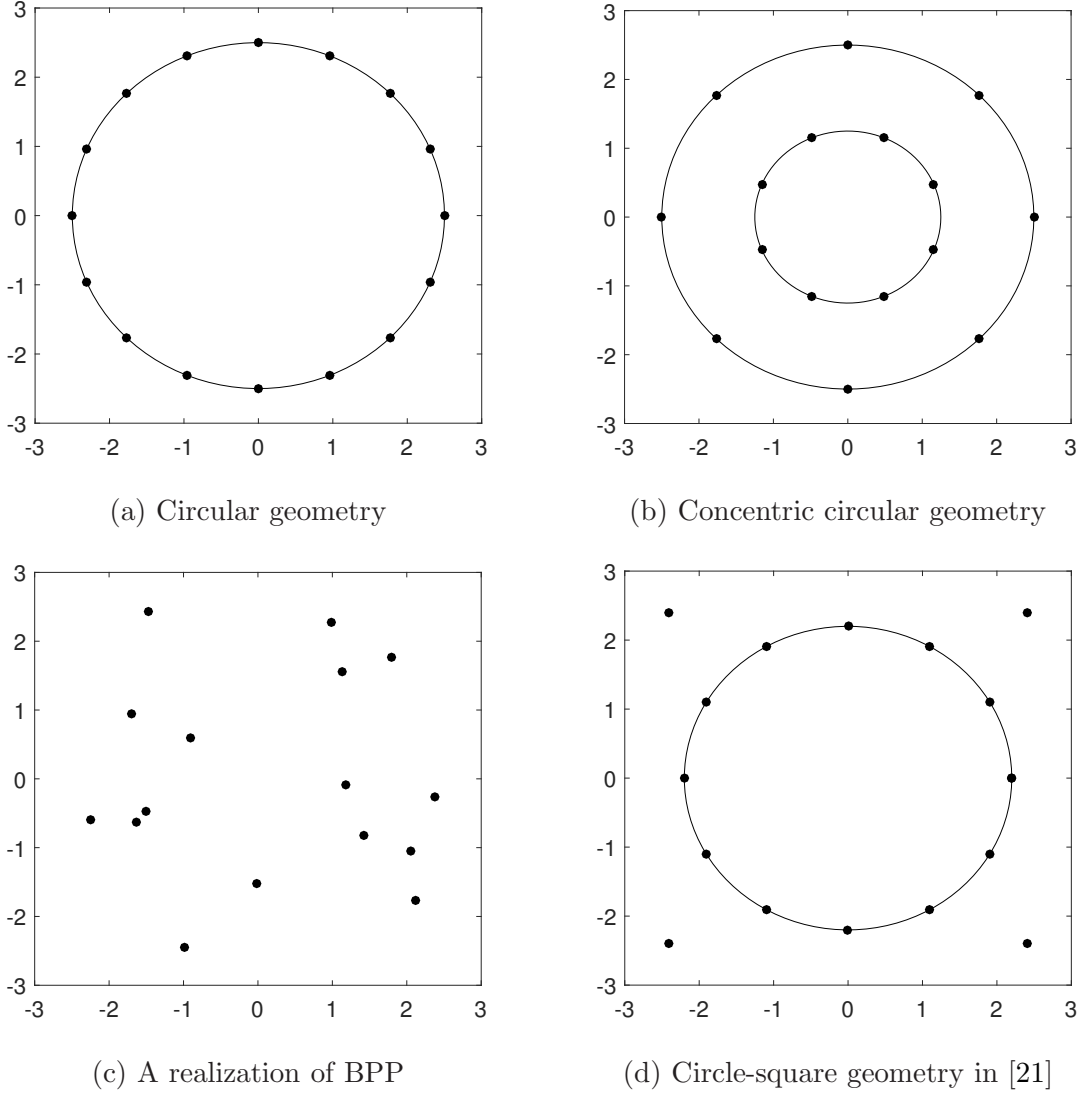
Figure 3.1: Arrangement of LEDs for different geometries

such cases, one possible way to obtain uniform illumination is through optimal power allocation by using the statistics of the BPP.

3.2 Power allocation for a BPP array

For a BPP, each LED is at a random location, so, heuristically, the power should also depend on the distance of the LED from the center of the array. The proposed power allocation is

$$P_{t_i} = \frac{r_i^{\alpha}}{\sum_{i=1}^{N} r_i^{\alpha}} P, \tag{3.1}$$

(a) Circular geometry

(b) Concentric Circular geometry

Figure 3.2: SNR distribution with equal power allocation

(a) With equal power allocation and optimal location

(b) With optimal power allocation and optimal location
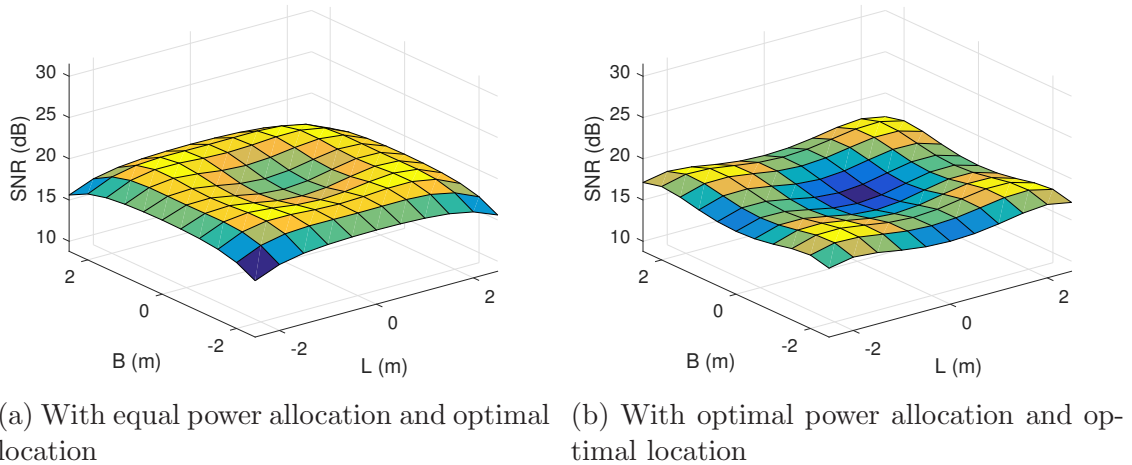
Figure 3.3: SNR distribution for circle-square geometry
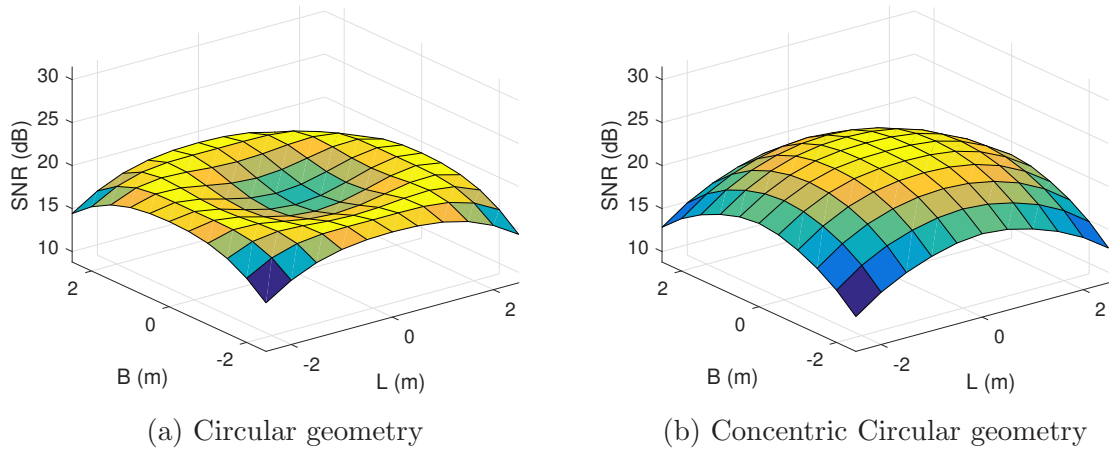
where P is the total source power, r_i is the location of the ith LED from the center, α is a suitable exponent and P_{t_i} is the power allocated to the ith LED. The heuristic in (3.1) makes the power allocation sub-optimal. For a BPP,

$$\Lambda_j = \mathbb{E}_\Phi \left[\frac{P_{r_j}}{\sigma_j^2} \right] \tag{3.2}$$

where $\mathbb{E}_\Phi$ is the expectation with respect to the BPP. Here we are looking at the illumination, hence $P_{r_j} = \sum_{i=1}^N H_{ij} P_{t_i}$. Plotting the quality factor $F_\Lambda(\alpha)$ in (2.14) with respect to α in Fig. 3.4, $F_\Lambda(\alpha)$ appears to be concave and has a maximum. An

15

Table 3.1: Simulation parameters

Parameters	Symbol	Configuration
Room size	$L \times B \times D$	$5m \times 5m \times 3m$
Height of receiver plane	h_r	$0.85m$
LED semi angle	$\phi_{\frac{1}{2}}$	60°

optimal value of α can then be obtained as

$$\max_{\alpha} F_{\Lambda}(\alpha), \tag{3.3}$$
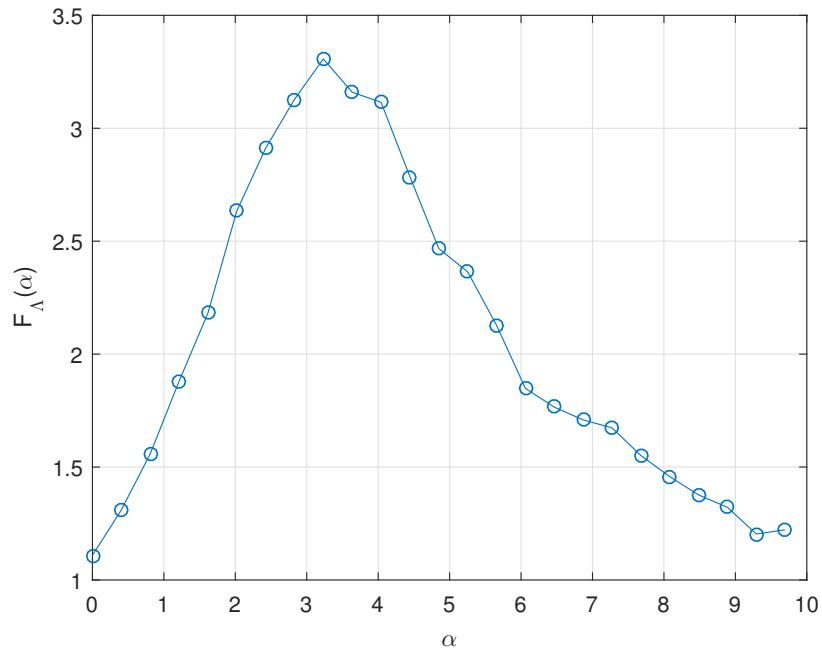
Figure 3.4: $F_{\Lambda}(\alpha)$ has a maximum

3.2.1 Algorithm for optimal α

The golden section search algorithm [29] in Fig. 3.6 is used for finding the optimum value of α in (3.1)
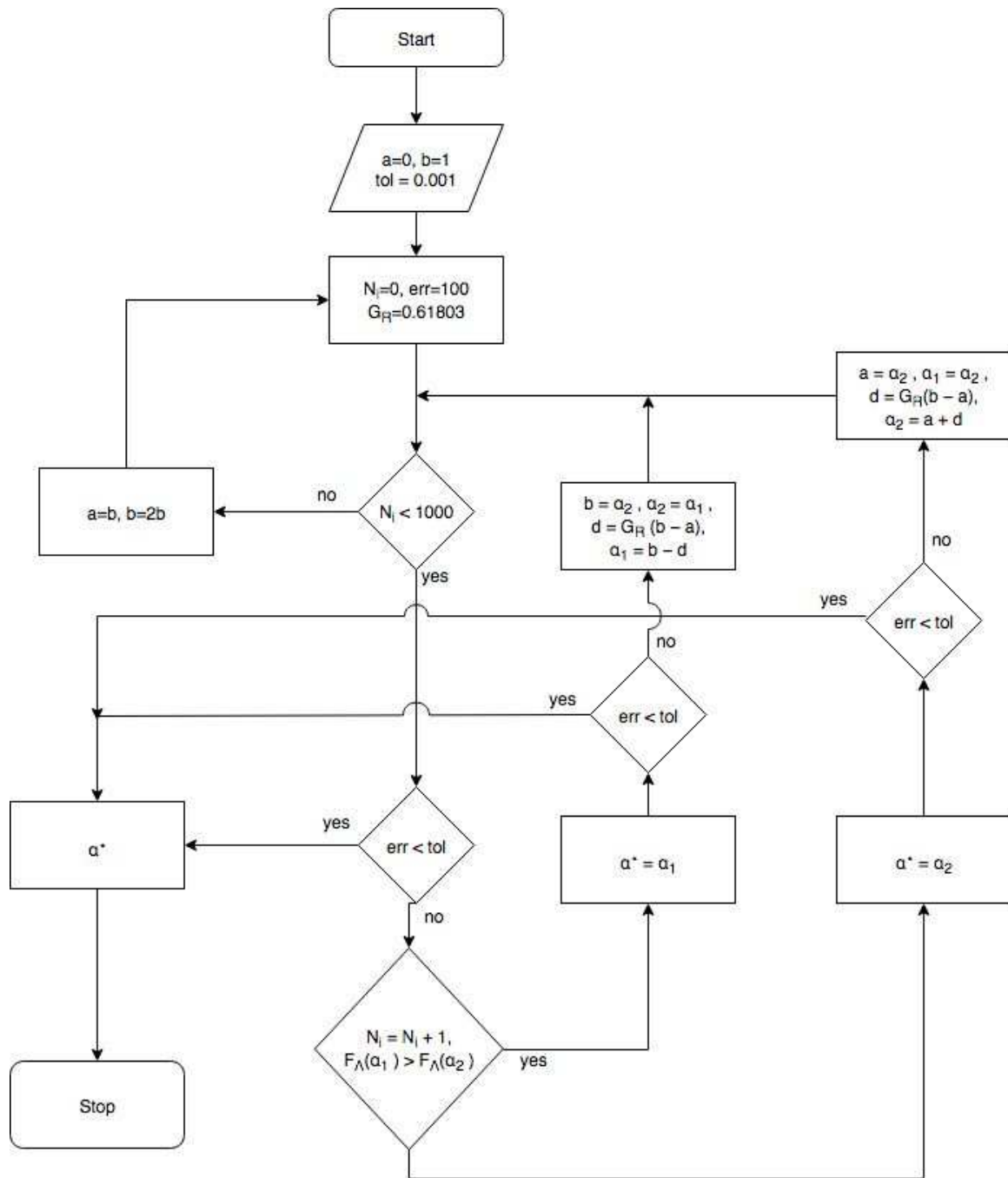
Figure 3.5: Golden section search algorithm

3.3 Results

The simulation parameters for the results obtained in this section are available in Tables 2.2 and 6.1 and are similar to those used in [21] and [26]. A simple search routine for maximizing $F_\Lambda(\alpha)$ in (2.14) using Fig. 3.4 results in $\alpha \approx 3.1$. The value
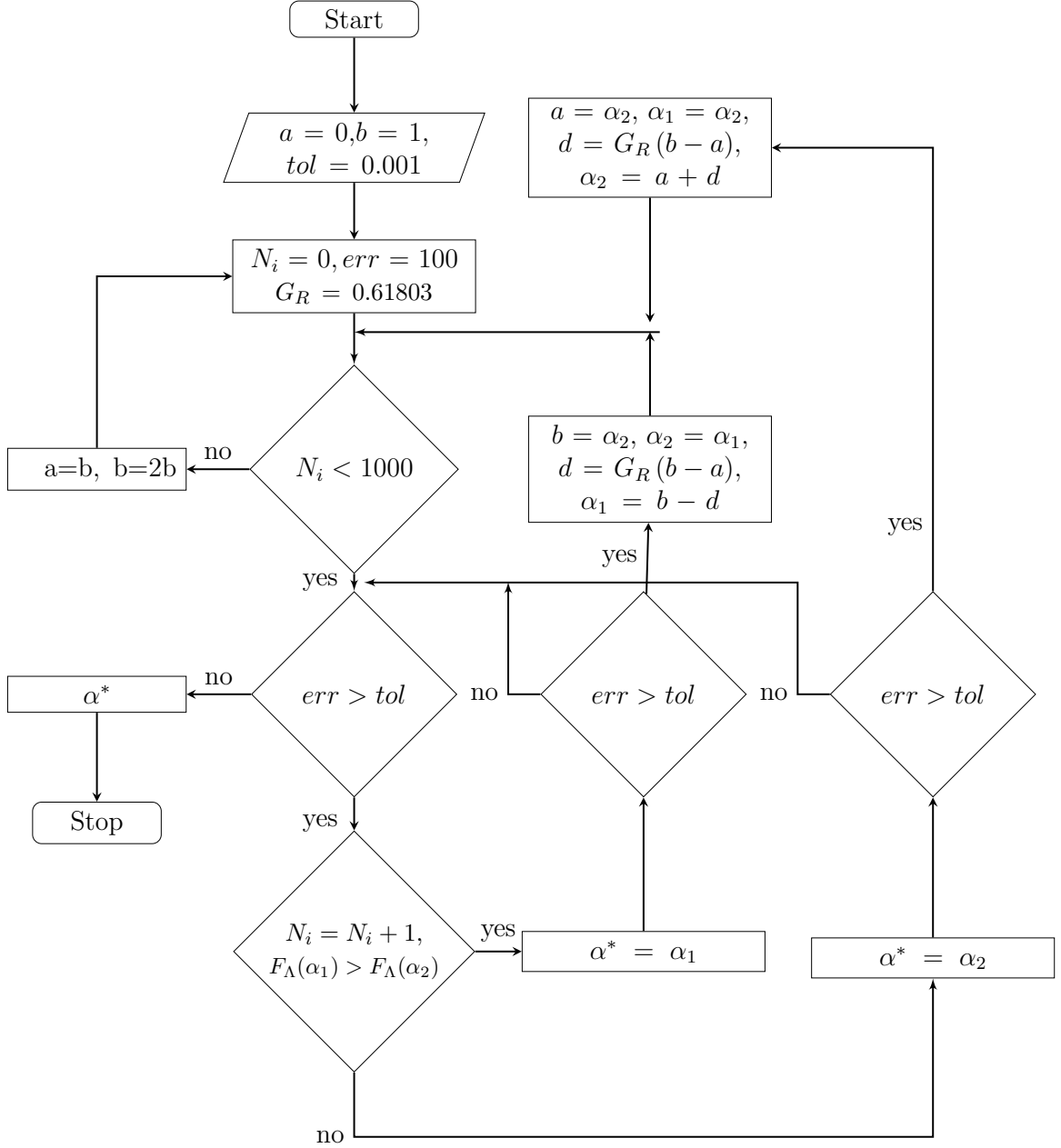
Figure 3.6: Golden section search algorithm

remains unchanged for higher values of N. This value is used in (3.2) and (3.1) to calculate the SNR profile. Figure 3.7 shows the SNR profiles calculated using (3.2) with and without power allocation for the BPP in Fig. 3.1c. The SNR profile for $N = 64$ for two different BPP realizations with sub-optimal power allocation is provided in Fig. 3.8. From Fig. 3.8, it is obvious that the heuristic power allocation scheme in (3.1) results in a uniform SNR profile. Also, the F_Λ value in Table 3.2 for the BPP in Fig. 3.1c is close to that of the circle-square array in Fig. 3.1d, indicating

(a) Equal power allocation

(b) Sub-optimal power allocation (3.1)
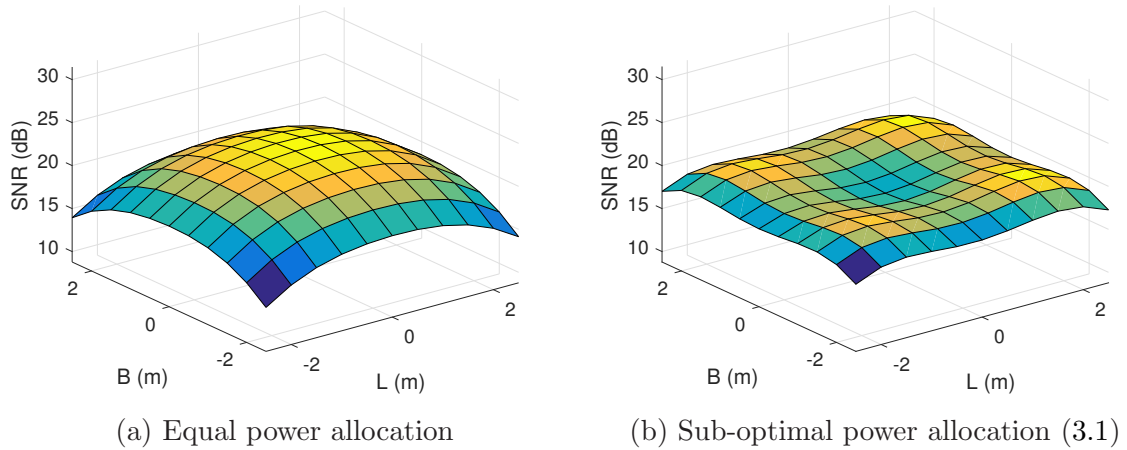
Figure 3.7: Average SNR for a BPP. $N = 16$

Table 3.2: SNR performance

	Circle-square		BPP	
	Equal Power	Optimal Power	Equal Power	Proposed heuristic
$\overline{\Lambda}\,(dB)$	18.2658	17.3447	20.1121	18.8510
$\mathrm{var}\,(\Lambda)\,(dB)$	21.4585	17.8065	33.5970	21.1082
F_Λ	2.8355	3.4924	1.0723	3.3780

that the BPP with even sub-optimal power allocation performs as well as a fixed geometry with optimal power allocation.
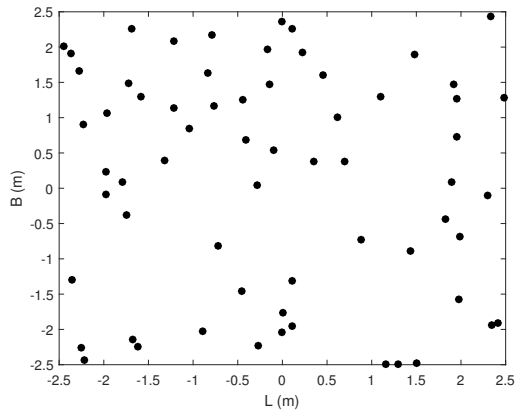
(a) $N = 64$, BPP realization 1
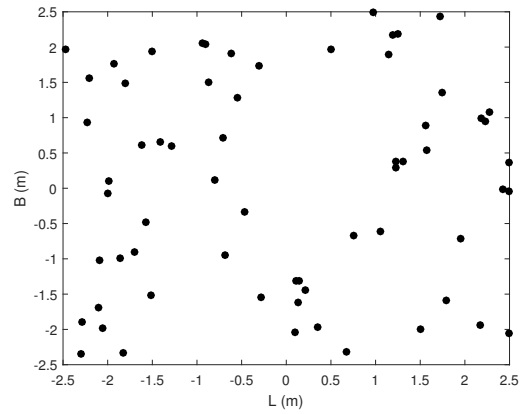
(b) $N = 64$, BPP realization 2
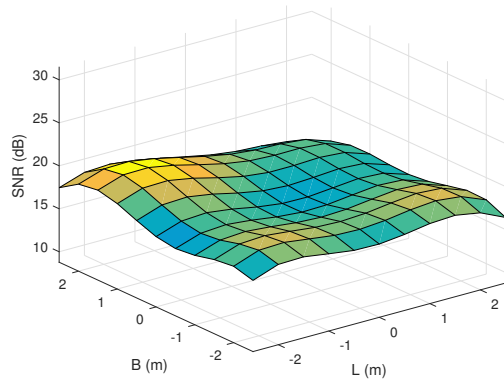
(c) SNR profile for realization 1
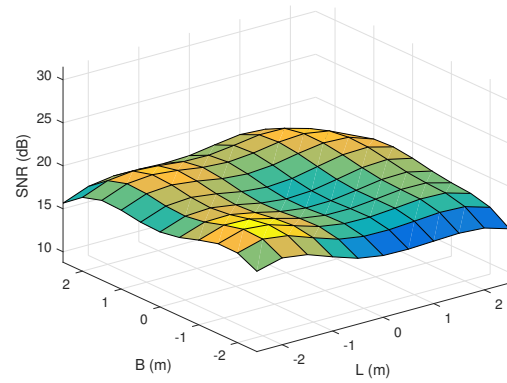
(d) SNR profile for realization 2

Figure 3.8: SNR for two different realizations for $N = 64$

Chapter 4

Resource Allocation for Visible Light Communication using Stochastic Geometry

A significant amount of research work has been done recently on using traditional light sources for wireless communication. Traditional digital communication and well-known wireless techniques have been applied in designing such a VLC system. Some of the notable systems are listed below:

- The performance of MIMO VLC is analyzed for different equalizers [30].

- An LED inclined MIMO (LIM) model is proposed and compared with an LED vertical MIMO (LVM) [31].

- The angular diversity is obtained by placing multiple photodetectors on a receiver node with a curved surface [32].

- Equalization is employed at the receiver to improve the data rate [33].

- An expression for the BER in the presence of interference is obtained [26].

4.1 Modeling light sources using stochastic geometry

In [21], BER performance analysis is done by considering a fixed LED array with optimal power allocation. Such results for VLC are rare and usually restricted to

light sources with a fixed geometry. In [21, 34], geometries of different kinds like square, circular and hexagonal models are studied. Stochastic geometry can be used for modeling all such geometries. Since each realization of a random geometry gives different SNR profiles, we look at an average SNR profile and BER. In [25], a heuristic power allocation was proposed and an average SNR was evaluated by averaging the SNR of each realization over the BPP. It was shown to achieve uniformity for a random geometry in an average sense. This can be observed in Fig. 4.1b for a square BPP. In [21], the BER expression of bipolar on-off keying (OOK) modulated signal for a fixed geometry is given by $Q(\sqrt{SNR})$. For a stochastic geometry, the average BER is calculated by averaging the BER of each realization over the BPP process Φ, $\mathbb{E}_{\Phi}[Q(\sqrt{SNR})]$. The BER curves obtained from simulations at the center of the geometry are plotted in Fig. 4.2 for various geometries. The average BER for stochastic geometry *appears to be close* to that for a fixed geometry, indicating that stochastic geometry can be used for modeling a VLC and the average BER of a BPP can be used for estimating system parameters.

In [25], the power allocation ensures the uniform illumination in the average sense, it would be interesting to find the optimum power allocation for a single realization of a random geometry.
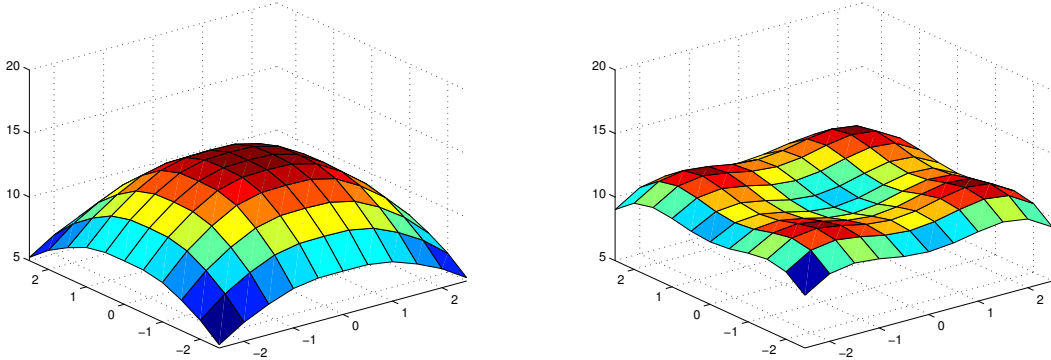
(a) Square array with equal power allocation (b) Square BPP with heuristic power allocation in (3.1)

Figure 4.1: SNR distribution with total power of 2 Watts

In this Chapter, the light sources are modeled using stochastic geometry [25], accounting for all possible source configurations. Thus, based on this theoretical model, it is possible to obtain estimates for the number of LED sources and their power consumption. This is useful for designing practical VLC systems using OOK modulation for an indoor environment where the light intensity is uniform [21]. Two stochastic
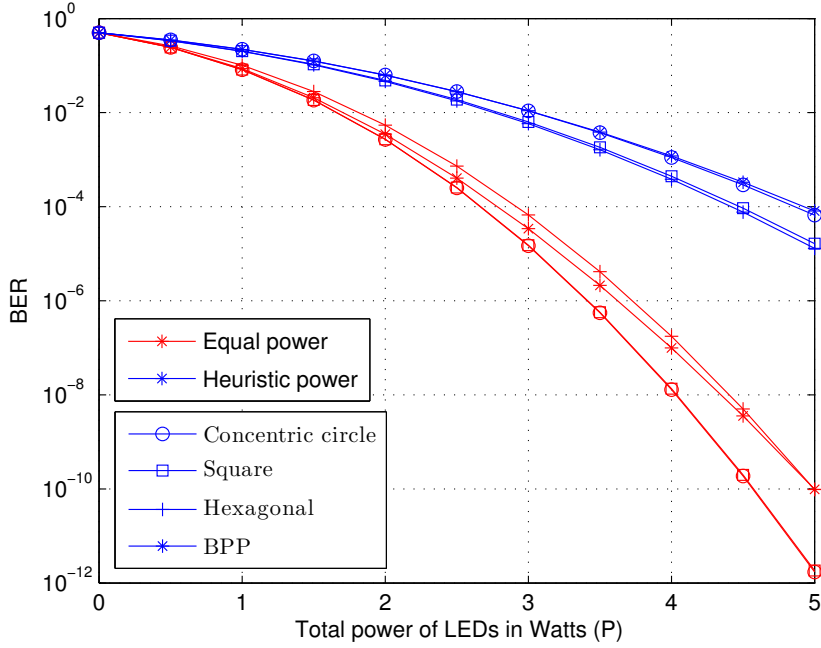
Figure 4.2: Simulated BER curves for various geometries with different power allocation schemes.

models are considered, square BPP and circular BPP. For a square BPP, which is the most appropriate stochastic model for an indoor environment, an expression for the average asymptotic BER is obtained. The asymptotic BER for a circular BPP is obtained in closed form. These help to provide reasonable estimates for the cost of the VLC system. In [25], a heuristic power allocation scheme was proposed for a BPP-VLC and shown to provide uniform irradiance on an average. To incorporate uniform irradiance into the VLC model in this paper, the same scheme is considered and described in the following section.

4.2   Power Allocation for a BPP array

The transmit power at the ith transmitter is given by the heuristic [25]

$$P_{t_i} = \frac{r_i^\alpha}{\sum_{j=1}^N r_j^\alpha} P, \tag{4.1}$$

where P is the total power allocated to the source, r_i is the distance of the ith LED from the center of the BPP in Fig. 2.3 and α is a constant.

4.3 BER Analysis

It has been shown in [25] that the power allocation scheme in (3.1) results in average uniform illumination. Thus, it is sufficient to obtain the BER at the photodetector located at the center [21], since uniform illumination results in the same signal strength at all photo-detectors at the receiver.We assume all the source LEDs transmit the same symbol x. From (2.6), the received symbol at the central photo-detector is

$$y_0 = RP_{r_0} + n_0 \tag{4.2}$$

From (2.7) and Table 2.1,

$$
\begin{aligned}
P_{r_0} &= \sum_{i=1}^{N} H_{i0} P_{t_i} M_I x \\
&= \sum_{i=1}^{N} \frac{P_{t_i} (m+1) A h^{m+1} x}{2\pi \left(\sqrt{h^2 + r_i^2} \right)^{m+3}} \\
&= \sum_{i=1}^{N} \frac{P M_I (m+1) A h^{m+1} r_i^{\alpha} x}{2\pi \left(\sum_{j=1}^{N} r_j^{\alpha} \right) \left(\sqrt{h^2 + r_i^2} \right)^{m+3}}
\end{aligned}
\tag{4.3}
$$

upon substituting for P_{t_i} from (3.1). Letting

$$
\begin{aligned}
C_1 &= \frac{P M_I (m+1) A h^{m+1}}{2\pi} \\
V_i &= \frac{r_i^{\alpha}}{\left(\sum_{j=1}^{N} r_j^{\alpha} \right) \left(\sqrt{h^2 + r_i^2} \right)^{m+3}},
\end{aligned}
\tag{4.4}
$$

P_{r_0} in (4.3) can be expressed as

$$P_{r_0} = C_1 \sum_{i=1}^{N} V_i \tag{4.5}$$

Substituting (4.5) in (4.2),

$$y_0 = \left(R C_1 \sum_{i=1}^{N} V_i \right) x + n_0 \tag{4.6}$$

24

Table 4.1: Simulation Parameters

Parameters	Symbol	Configuration
Room size	$L \times B \times D$	$5m \times 5m \times 3m$
Height of receiver plane	h_r	$0.85m$
Modulation index	M_I	0.2
LED semiangle	$\phi_{\frac{1}{2}}$	60°

Since n_0 is AWGN, the conditional BER for the BPP can be obtained from (4.6) as

$$P_e = Q\left(\frac{RC_1 \sum_{i=1}^{N} V_i}{\sigma_0}\right) \qquad (4.7)$$

where $Q(.)$ is the Q-function, defined as [35]

$$Q(x) = \frac{1}{\sqrt{2\pi}} \int_x^\infty e^{-x^2/2} dx, \quad x \geq 0. \qquad (4.8)$$

4.4   Asymptotic BER

Theorem 4.4.1. For any point process based VLC, an asymptotic (large N) expression for BER is given by

$$P_e = Q\left(\frac{RC_1 \sum_{i=1}^{N} \mathbb{E}_\Phi[V_i]}{\sqrt{\mathbb{E}_\Phi[\sigma_0^2]}}\right) \qquad (4.9)$$

where [25]

$$\sigma_0^2 = 2qRM_IC_1 \sum_{i=1}^{N} V_iB + 2qI_{bg}I_2B + \frac{8\pi kT_k}{G}\eta AI_2B^2 + \frac{16\pi^2 kT_k\Gamma}{g_m}\eta^2 A^2 I_3 B^3 \quad (4.10)$$

Proof. See Appendix 4.6.1. ∎

Since $\mathbb{E}_\Phi[\sigma_0^2]$ is dependent on $\mathbb{E}_\Phi[V_i]$, the latter needs to be evaluated to obtain an expression for P_e in (4.9).

Corollary 4.4.2. For square and circular BPPs, $\mathbb{E}_\Phi[V_i]$ is given by (4.11) and (4.13) respectively.

Proof. See Appendix 4.6.2. ∎

25

Square BPP:

$$\mathbb{E}_{\Phi}\left[V_i\right] = \frac{R_i^{\alpha}}{\mathcal{B}\left(N-i+1,i\right)\sum_{j=1}^{N}\mathbb{E}_{\Phi}\left[r_j^{\alpha}\right]}\sum_{k=0}^{N-i}\frac{\binom{N-i}{k}(-1)^k\left(R_i^2\right)^{k+i}}{W^{k+i}}$$

$$\times\left[\frac{(\pi)^{k+i}}{h^{m+3}\left(k+i+\alpha/2\right)}\,{}_2F_1\left(\frac{m+3}{2},k+i+\alpha/2;k+i+\alpha/2+1;-\frac{R_i^2}{h^2}\right)+\right.$$

$$\left.\int_0^{\frac{\pi}{4}}\frac{2\left(\pi-4\theta\right)\left(\pi-4\theta+2\sin\left(2\theta\right)\right)^{k+i-1}}{R_i cos^{2(k+i-2)+\alpha-m}\left(\theta\right)\left(\sqrt{R_i^2+h^2cos^2\left(\theta\right)}\right)^{m+3}}\right] \quad (4.11)$$

where

$$\mathbb{E}_{\Phi}\left[r_i^{\alpha}\right]=\frac{1}{\mathcal{B}\left(N-i+1,i\right)}\sum_{k=0}^{N-i}\frac{\binom{N-i}{k}(-1)^k R_i^{2(k+i)+\alpha}}{W^{k+i}}\left[\frac{\pi^{k+i}}{k+i+\alpha/2}\right.$$

$$\left.+\int_0^{\frac{\pi}{4}}\frac{2\left(\pi-4\theta\right)\left(\pi-4\theta+2\sin\left(2\theta\right)\right)^{k+i-1}}{R_i\cos^{2(k+i)+\alpha-1}\left(\theta\right)}\,d\theta\right] \quad (4.12)$$

Circular BPP:

$$\mathbb{E}_{\Phi}\left[V_i\right]=\frac{R_c^{\alpha}}{h^{m+3}\mathcal{B}\left(N-i+1,i\right)\sum_{j=1}^{N}\mathbb{E}_{\Phi}\left[r_j^{\alpha}\right]}$$

$$\times\sum_{k=0}^{N-i}\frac{\binom{N-i}{k}(-1)^k}{\left(i+k+\frac{\alpha}{2}\right)}\,{}_2F_1\left(\frac{m+3}{2},i+k+\frac{\alpha}{2};i+k+\frac{\alpha}{2}+1;-\frac{R_c^2}{h^2}\right),$$

$$(4.13)$$

$$\mathbb{E}_{\Phi}\left[r_i^{\alpha}\right]=\frac{R_c^{\alpha}}{\mathcal{B}\left(N-i+1,i\right)}\sum_{k=0}^{N-i}\frac{\binom{N-i}{k}(-1)^k}{\left(i+k+\frac{\alpha}{2}\right)} \quad (4.14)$$

Table 4.2: Power Allocation and Irradiance Metric

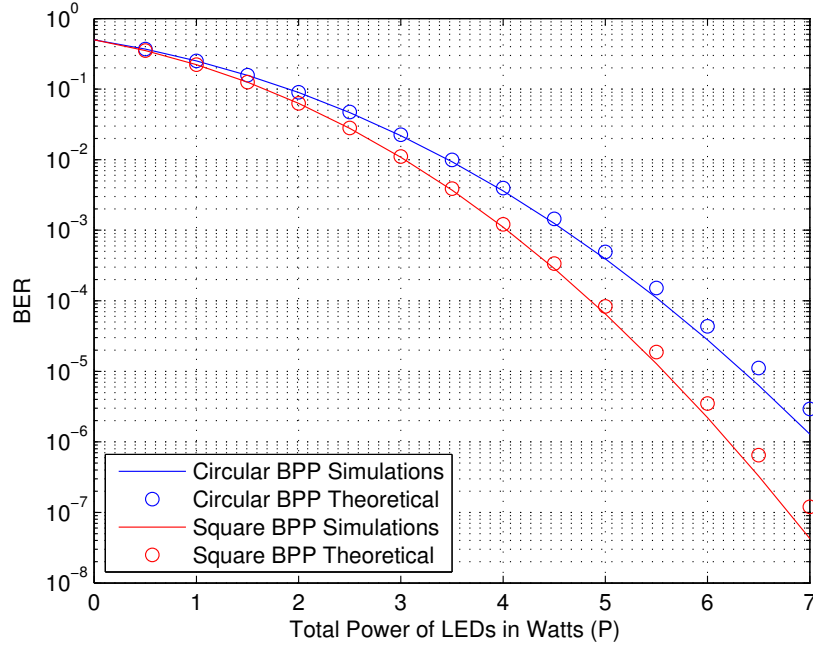| Geometry	$F_{\Lambda}\left(\alpha\right)$	α
Square Array[4]	2.16	0
Square BPP	3.36	3.1
Circular BPP	4.07	1.2

Figure 4.3: BER for various geometries

4.5   Results

All the physical parameters for the system have been obtained from [11] and Table 6.1. $\alpha = 3.2, 1.2$ for square and circular geometries. The asymptotic BER obtained in (4.9) is plotted for square and circular BPP in Fig. 4.3. The simulations are obtained for large number of source LEDs for N=50. The asymptotic BER expression is validated and matches well with the simulation results.

In Fig. 5.3 the asymptotic BER obtained in (4.9) is plotted for different geometries. Analytical expressions are used for the circular BPP. For the square array, simulation results are available in Fig. 5.3. Fig. 5.3 also shows that for a given BER, the power requirements for a regular array can be estimated using the asymptotic BER expression for a stochastic array in (4.9) since the BER curves are not too far off. For example, for a BER of 10^{-6}, the power requirement for the circular BPP is 7W, whereas the requirement for a regular square array is 5W. Thus, it is reasonable to consider power consumption by the circular BPP as an upper limit on the actual power requirement for any array.

Fig. 5.4 shows the simulated BER behavior for all geometries with increasing number of LEDs. The power consumption is assumed to be 4W. It is obvious from the figure that after $N = 20$, the actual BER performance is close to the asymptotic
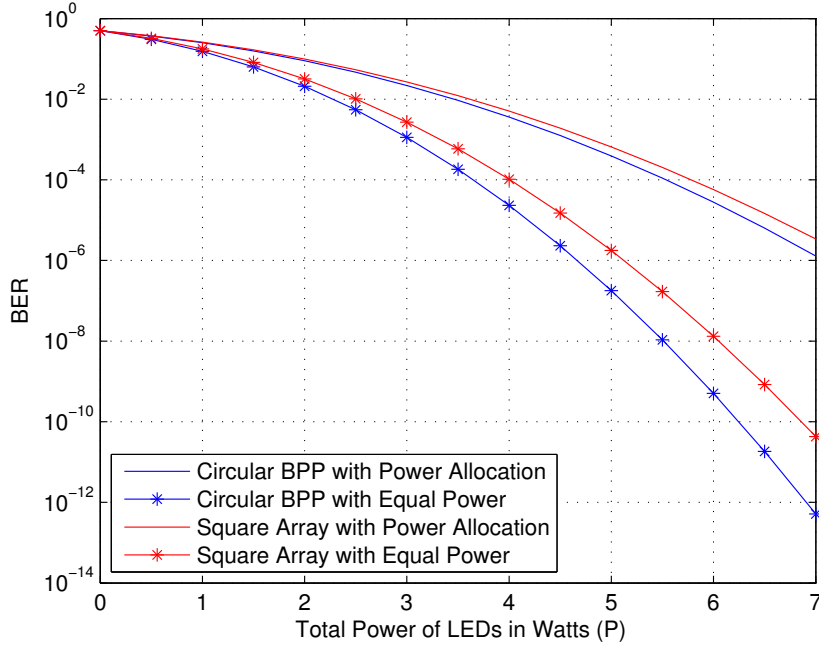
27

Figure 4.4: Analytical BER plot of the circular BPP is close to a square array.

BER. Also, the shape of the simulated BER curves for circular and square geometries is similar. Thus, the closed form BER expression for the asymptotic BER can be used to estimate the cost of the system in terms of the number of LEDs. However, as can be seen from Fig. 4.5, a graphical, but intuitive approach is required for this.

4.6 Appendix

4.6.1 Proof for asymptotic BER

Unconditioning (4.7),

$$P_e = \mathbb{E}_\Phi \left[Q \left(\frac{RC_1 \sum_{i=1}^N V_i}{\sigma_0} \right) \right] \tag{4.15}$$

Jensens Inequality: If X is a random variable (RV) and f is a convex function, then [36, (9.1.3)],

$$f\left(\mathbb{E}\left[X \right] \right) \leq \mathbb{E}\left[f\left(X \right) \right] \tag{4.16}$$

Using (4.16) in (4.15),

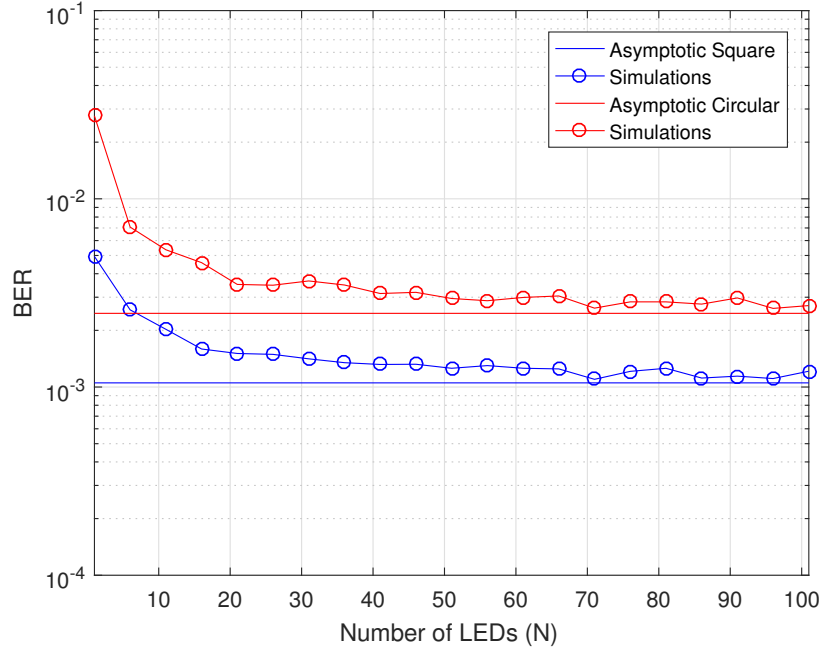$$P_e \geq Q \left(\mathbb{E}_\Phi \left[\frac{RC_1 \sum_{i=1}^N V_i}{\sigma_0} \right] \right) \tag{4.17}$$

Figure 4.5: Simulated BER matches the theoretical asymptotic BER for large N.

since $Q\left(\cdot\right)$ is convex.

Lemma 4.6.1. Consider random variables X and Y where Y either has no mass at 0 (discrete) or has support $[0, \infty)$. Then [37], [38]

$$\mathbb{E}\left[f\left(X, Y\right)\right] \approx f\left(\mathbb{E}\left[X\right], \mathbb{E}\left[Y\right]\right) \tag{4.18}$$

Corollary 4.6.1.

$$\mathbb{E}\left[\frac{X}{Y}\right] \approx \frac{\mathbb{E}\left[X\right]}{\mathbb{E}\left[Y\right]} \tag{4.19}$$

$$\mathbb{E}\left[X^2\right] \approx \left(\mathbb{E}\left[X\right]\right)^2 \tag{4.20}$$

Since $\sigma_0 > 0$, using (4.19) and (4.20) in (4.17),

$$Q\left(\mathbb{E}_\Phi\left[\frac{RC_1 \sum_{i=1}^N V_i}{\sigma_0}\right]\right) \approx Q\left(\frac{RC_1 \sum_{i=1}^N \mathbb{E}_\Phi\left[V_i\right]}{\mathbb{E}_\Phi\left[\sigma_0\right]}\right)$$

$$= Q\left(\frac{RC_1 \sum_{i=1}^N \mathbb{E}_\Phi\left[V_i\right]}{\sqrt{\mathbb{E}_\Phi\left[\sigma_0^2\right]}}\right) \tag{4.21}$$

29

resulting in

$$P_e \gtrapprox Q\left(\frac{RC_1 \sum_{i=1}^{N} \mathbb{E}_\Phi\left[V_i\right]}{\sqrt{\mathbb{E}_\Phi\left[\sigma_0^2\right]}}\right) \tag{4.22}$$

4.6.2 Derivation of $\mathbb{E}_\Phi\left[V_i\right]$

BER Analysis for Square BPP

For a BPP distributed over a square region of area A, the pdf of the distance to the ith nearest node from the origin is [28]

$$f_{r_i} = \begin{cases} \frac{2\pi r}{W} \frac{(1-p)^{N-i} p^{i-1}}{\mathcal{B}(N-i+1,i)} & 0 < r < R_i \\ \frac{2(\pi-4\theta)r}{W} \frac{(1-q)^{N-i} q^{i-1}}{\mathcal{B}(N-i+1,i)} & R_i < r < R_c \\ 0 & R_c < r \end{cases} \tag{4.23}$$

where $\theta = \cos^{-1}(R_i/r)$, $p = \frac{\pi r^2}{A}$, $q = \frac{\pi r^2 - 4r^2\theta + 2r^2 \sin(2\theta)}{A}$, R_i and R_c are the radii of the incircle and circumcircle of A.

$$\mathbb{E}_\Phi\left[r_i^\alpha\right] = \int_{-\infty}^{\infty} r^\alpha f_{r_i}(r) dr \tag{4.24}$$

$$= \int_0^{R_i} r^\alpha \frac{2\pi r}{W} \frac{(1-p)^{N-i} p^{i-1}}{\mathcal{B}(N-i+1,i)} dr + \int_{R_i}^{R_c} r^\alpha \frac{2(\pi-4\theta)r}{W} \frac{(1-q)^{N-i} q^{i-1}}{\mathcal{B}(N-i+1,i)} dr$$

$$= \mathcal{I}_1 + \mathcal{I}_2$$

where

$$\mathcal{I}_1 = \int_0^{R_i} r^\alpha \frac{2\pi r}{W} \frac{(1-p)^{N-i} p^{i-1}}{\mathcal{B}(N-i+1,i)} dr$$

$$= \frac{2\pi}{W\mathcal{B}(N-i+1,i)} \sum_{k=0}^{N-i} \binom{N-i}{k} (-1)^k \left(\frac{\pi}{W}\right)^{k+i-1} \int_0^{R_i} r^{2(k+i+\alpha/2+1/2)} dr$$

$$= \frac{1}{\mathcal{B}(N-i+1,i)} \sum_{k=0}^{N-i} \frac{\binom{N-i}{k}(-1)^k}{k+i+\alpha/2} \left(\frac{\pi}{W}\right)^{k+i} R_i^{2(k+i)+\alpha}$$

$$\mathcal{I}_2 = \int_{R_i}^{R_c} r^\alpha \frac{2(\pi-4\theta)r}{W} \frac{(1-q)^{N-i} q^{i-1}}{\mathcal{B}(N-i+1,i)} dr$$

$$= \frac{1}{\mathcal{B}(N-i+1,i)} \sum_{k=0}^{N-i} \frac{\binom{N-i}{k}(-1)^k}{W^{k+i}} R_i^{2(k+i)+\alpha-1}$$

$$\times \int_0^{\frac{\pi}{4}} \frac{2(\pi-4\theta)(\pi-4\theta+2\sin(2\theta))^{k+i-1}}{\cos^{2(k+i)+\alpha-1}(\theta)} d\theta$$

30

upon substituting $R_i = r \cos \theta$. For simplifying the analysis, using the approximation

$$\sum_{j=1}^{N} \mathbb{E}_{\Phi} \left[r_j^{\alpha} \right] \approx \sum_{j=1}^{N} r_j^{\alpha}$$

in (4.4),

$$\mathbb{E}_{\Phi} \left[V_i \right] = \frac{1}{\sum_{j=1}^{N} \mathbb{E}_{\Phi} \left[r_j^{\alpha} \right]} \mathbb{E}_{\Phi} \left[\frac{r^{\alpha}}{\left(\sqrt{r^2 + h^2} \right)^{m+3}} \right]$$

$$= \frac{\mathcal{J}_1 + \mathcal{J}_2}{\sum_{j=1}^{N} \mathbb{E}_{\Phi} \left[r_j^{\alpha} \right]}$$

where

$$\mathcal{J}_1 = \int_0^{R_i} \frac{r^{\alpha}}{\left(\sqrt{r^2 + h^2} \right)^{m+3}} \frac{2\pi r}{W} \frac{(1-p)^{N-i} p^{i-1}}{\mathcal{B}(N-i+1,i)} dr$$

$$= \frac{R_i^{\alpha}}{h^{m+3} \mathcal{B}(N-i+1,i)} \sum_{k=0}^{N-i} \binom{N-i}{k} (-1)^k \left(\frac{\pi R_i^2}{W} \right)^{k+i} \int_0^{R_i^2/h^2} \frac{t^{(k+i+\alpha/2)-1}}{(1+t)^{\frac{m+3}{2}}} dt$$

(4.25)

after some algebra. From [39],

$$\int_0^u \frac{x^{\mu-1}}{(1+\beta x)^{\nu}} dx = \frac{u^{\mu}}{\mu} \, {}_2F_1 \left(\nu, \mu; 1+\mu; -\beta u \right) \, [|arg\,(1+\beta u)| < \pi, Re\mu > 0]$$

Substituting the above in (4.25),

$$\mathcal{J}_1 = \frac{h^{\alpha-(m+3)}}{\mathcal{B}(N-i+1,i)} \sum_{k=0}^{N-i} \binom{N-i}{k} (-1)^k \left(\frac{\pi h^2}{W} \right)^{k+i}$$

$$\times \, {}_2F_1 \left(\frac{m+3}{2}, k+i+\frac{\alpha}{2}, k+i+\frac{\alpha}{2}+1; -\frac{R_i^2}{h^2} \right)$$

Similarly,

$$\mathcal{J}_2 = \int_{R_i}^{R_c} \frac{r^{\alpha+1} 2\,(\pi-4\theta)}{W \left(\sqrt{r^2+h^2} \right)^{m+3}} \frac{(1-q)^{N-i} q^{i-1}}{\mathcal{B}(N-i+1,i)} dr$$

$$= \frac{1}{\mathcal{B}(N-i+1,i)} \sum_{k=0}^{N-i} \frac{\binom{N-i}{k} (-1)^k}{W^{k+i}}$$

31

$$\times \int_0^{\frac{\pi}{4}} \frac{2\left(\pi-4\theta\right)R_i^{2(k+i)+\alpha-1}}{\left(\cos\theta\right)^{2(k+i-2)+\alpha-m}} \frac{\left(\pi-4\theta+2\sin\left(2\theta\right)\right)^{k+i-1}}{\left(\sqrt{R_i^2+h^2\cos^2\left(\theta\right)}\right)^{m+3}}d\theta \qquad \blacksquare$$

BER analysis for circular BPP

The probability density function (PDF) of the distance of ith nearest LED location from origin for circular BPP for $0 \le r \le R_c$ is given by [28]

$$f_{r_i} = \frac{2r}{R_c^2 \mathcal{B}(N-i+1,i)}\left(\frac{r^2}{R_c^2}\right)^{i-1}\left(1-\frac{r^2}{R_c^2}\right)^{N-i}$$

$$\Rightarrow \mathbb{E}_\Phi[r_i^\alpha] = \int_0^\infty r^\alpha f_{r_i}(r)dr$$

$$= \int_0^{R_c} \frac{2r^{\alpha+1}}{R_c^2\mathcal{B}(N-i+1,i)}\left(\frac{r^2}{R_c^2}\right)^{i-1}\left(1-\frac{r^2}{R_c^2}\right)^{N-i}dr$$

$$= \frac{1}{\mathcal{B}(N-i+1,i)}\sum_{k=0}^{N-i}\binom{N-i}{k}(-1)^k\int_0^{R_c^2}\frac{t^{i+k+\alpha/2-1}}{R_c^{2(i+k)}}dt$$

$$= \frac{R_c^\alpha}{\mathcal{B}(N-i+1,i)}\sum_{k=0}^{N-i}\frac{\binom{N-i}{k}(-1)^k}{\left(i+k+\frac{\alpha}{2}\right)} \qquad (4.26)$$

through a change of variables and using [39, (3.194)]

$$\mathbb{E}_\Phi[V_i] = \frac{1}{\sum_{j=1}^N \mathbb{E}_\Phi[r_j^\alpha]}\mathbb{E}_\Phi\left[\frac{r^\alpha}{\left(\sqrt{r^2+h^2}\right)^{m+3}}\right]$$

$$= \frac{1}{\sum_{j=1}^N \mathbb{E}_\Phi[r_j^\alpha]}\int_0^{R_c}\frac{2r}{\mathcal{B}(N-i+1,i)}\sum_{k=0}^{N-i}\binom{N-i}{k}\frac{(-1)^k r^{2(i+k+\alpha/2-1)}}{R_c^{2(i+k)}\left(\sqrt{r^2+h^2}\right)^{m+3}}dr$$

$$= \frac{1}{\mathcal{B}(N-i+1,i)\sum_{j=1}^N \mathbb{E}_\Phi[r_j^\alpha]}\int_0^{R_c^2/h^2}\sum_{k=0}^{N-i}\frac{\binom{N-i}{k}(-1)^k h^2 \left(h^2 t\right)^{(i+k+\alpha/2-1)}}{R_c^{2(i+k)}h^{m+3}\left(\sqrt{1+t}\right)^{m+3}}dt$$

$$= \frac{1}{\mathcal{B}(N-i+1,i)\sum_{j=1}^N \mathbb{E}_\Phi[r_j^\alpha]}$$
$$\times \sum_{k=0}^{N-i}\binom{N-i}{k}\frac{(-1)^k h^{2(i+k+\alpha/2)}}{h^{m+3}R_c^{2(i+k)}}\int_0^{R_c^2/h^2}\frac{t^{(i+k+\alpha/2-1)}}{(1+t)^{(m+3)/2}}dt$$

$$= \frac{R_c^\alpha h^{-(m+3)}}{\mathcal{B}(N-i+1,i)\sum_{j=1}^N \mathbb{E}_\Phi[r_j^\alpha]}$$
$$\times \sum_{k=0}^{N-i}\frac{\binom{N-i}{k}(-1)^k}{\left(i+k+\frac{\alpha}{2}\right)}{}_2F_1\left(\frac{m+3}{2},i+k+\frac{\alpha}{2};i+k+\frac{\alpha}{2}+1;-\frac{R_c^2}{h^2}\right) \qquad \blacksquare$$

Chapter 5

Asymptotic BER Performance of Circle-square Geometry in Visible Light Communication

The asymptotic BER performance of square BPP and circular BPP has been analyzed in previous chapter. Black spots are the regions where source LEDs cannot be placed at certain locations because of design restrictions in a room like fans, non-availability of electrical wiring etc.. Such cases can be modeled by approximating the square BPP with multiple non-overlapping circles. This process is referred as Circle-square BPP. In this chapter, the BER performance analysis of circle-square BPP is presented and compared with square BPP.

5.1   CDF and PDF of distance distribution

In order to derive the asymptotic BER, we need to find the distance distribution of Circle-square BPP process.

Theorem 5.1.1. The CDF F_{r_n} and PDF f_{r_n} of the distance to the nth neighbor from origin are

$$F_{r_n}(r) = \begin{cases} 0 & r < 0 \\ 1 - \sum_{k=0}^{n-1} \binom{N}{k} p^k (1-p)^{N-k} & 0 \le r \le \frac{L}{2} + 2k \\ 1 & r > \frac{L}{2} + 2k \end{cases} \tag{5.1}$$

$$f_{r_n}(r) = \frac{dp}{dr} \frac{(1-p)^{N-n} p^{n-1}}{\mathcal{B}(N-n+1, n)} \tag{5.2}$$

where

$$p = \begin{cases} \frac{r^2}{(L/2)^2 + 4k^2} & 0 < r < L/2 \\ \frac{\pi\left(\frac{L}{2}\right)^2 + 4\left(\theta_A r^2 + \theta_B k^2 - dy\right)}{\pi\left((L/2)^2 + 4k^2\right)} & L/2 < r < L/2 + 2k \\ 1 & r > L/2 + 2k \end{cases} \qquad (5.3)$$

$$\frac{dp}{dr} = \begin{cases} \frac{2r}{(L/2)^2 + 4k^2} & 0 < r < L/2 \\ \frac{4\left(\theta_A' r^2 + 2\theta_A r + \theta_B' k^2 - dy'\right)}{\pi\left((L/2)^2 + 4k^2\right)} & L/2 < r < L/2 + 2k \\ 0 & r > L/2 + 2k \end{cases} \qquad (5.4)$$

and

$$\theta_A = \cos^{-1}\left(\frac{x}{r}\right) \qquad \theta_B = \cos^{-1}\left(\frac{d-x}{k}\right) \qquad x = \frac{r^2 - k^2 + d^2}{2d} \qquad y = \sqrt{r^2 - x^2} \qquad (5.5)$$

$$\theta_A' = \frac{(x - rx')}{r\sqrt{r^2 - x^2}} \qquad \theta_B' = \frac{x'}{\sqrt{k^2 - y^2}} \qquad x' = \frac{r}{d} \qquad y' = \frac{r - xx'}{\sqrt{r^2 - x^2}} \qquad (5.6)$$
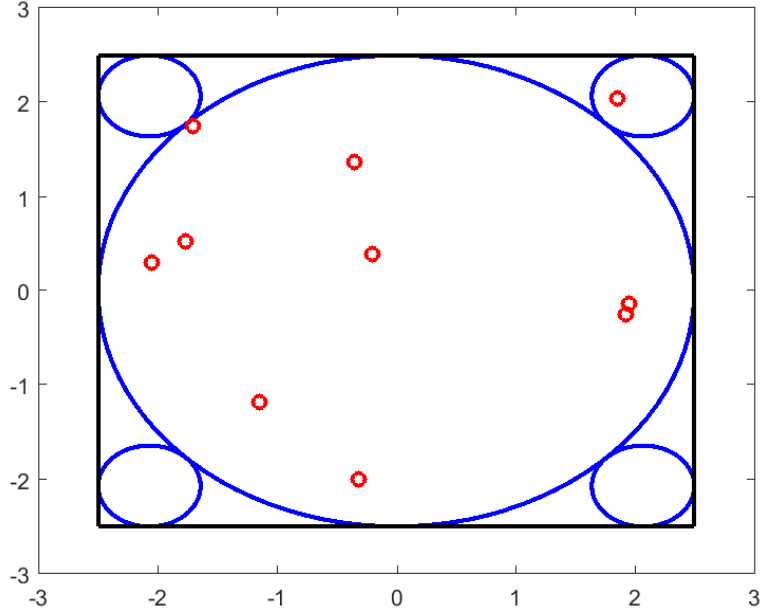
Proof. See Appendix 5.4.1

Figure 5.1: Realization of BPP with 10 LEDs

Table 5.1: Power allocation and irradiance metric

Geometry	$F_\Lambda(\alpha)$	α
Sqaure	1.08	0
Square	3.3	3.2
Circumcircle	4.07	1.2
Circle-square	3.27	4

5.2 BER Analysis

An asymptotic (large N) expression for BER for any point process based VLC is given by 4.9

$$P_e = Q\left(\frac{RC_1 \sum_{i=1}^N \mathbb{E}_\Phi[V_i]}{\sqrt{\mathbb{E}_\Phi[\sigma_0^2]}}\right) \tag{5.7}$$

Expressions for $\mathbb{E}_\Phi[V_i]$ and $\mathbb{E}_\Phi[\sigma_0^2]$ need to be evaluated to obtain an expression for P_e in (4.9). These are evaluated in the following section. The desired expressions for obtaining P_e for this geometry are given by (see Appendix 5.4.2)

$$\mathbb{E}_\Phi[r_i^\alpha] = \left(\frac{L}{2} + 2k\right)^\alpha - \alpha \int_0^{\frac{L}{2}+2k} r^{\alpha-1} F_{r_i}(r) dr \tag{5.8}$$

$$\mathbb{E}_\Phi[V_i] = \frac{1}{\sum_{j=1}^N \mathbb{E}_\Phi\left[r_j^\alpha\right]} \left[\frac{\left(\frac{L}{2} + 2k\right)^\alpha}{\left(\sqrt{\left(\frac{L}{2}+2k\right)^2 + h^2}\right)^{m+3}} \right. $$

$$\left. - \int_0^{\frac{L}{2}+2k} \frac{r^{\alpha-1}\left(r^2(\alpha-m-3)+h^2\alpha\right)F_{r_i}(r)}{\left(\sqrt{r^2+h^2}\right)^{m+5}} dr \right].$$

5.3 Results

All the physical parameters for the system have been obtained from [11]. α in (2.14) is numerically obtained and tabulated in Table 6.3 for different geometries. The irradiance profile for these geometries is then calculated using α in Table 6.3 and shown in Fig. 5.2. It is clear from the figure that random geometries can generate *near* uniform illumination with appropriate power allocation.
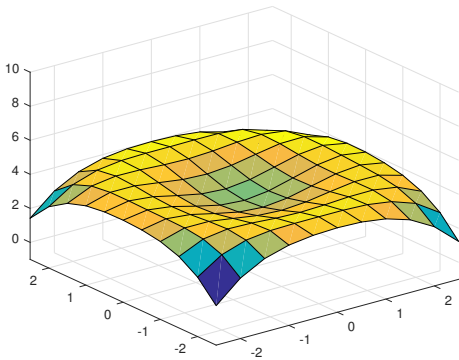
The asymptotic BER obtained in (4.9) for different geometries is plotted in Fig. 5.3 for $M_I = 0.2$. Analytical expressions are used for the circular and circle-square
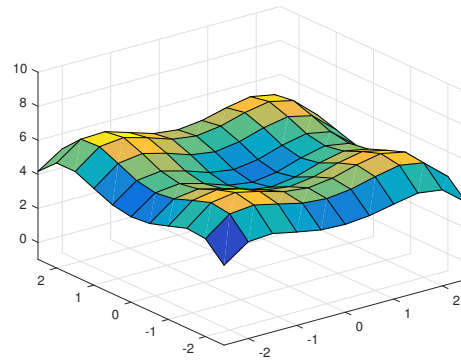
35
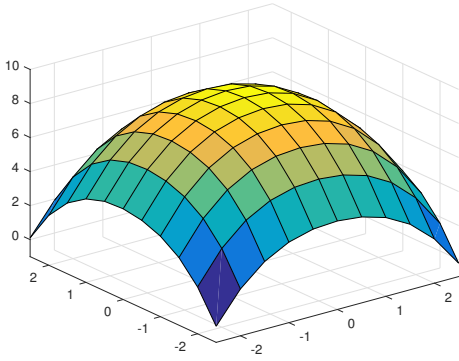
(a) Random Square Geometry Equal Power Allocation
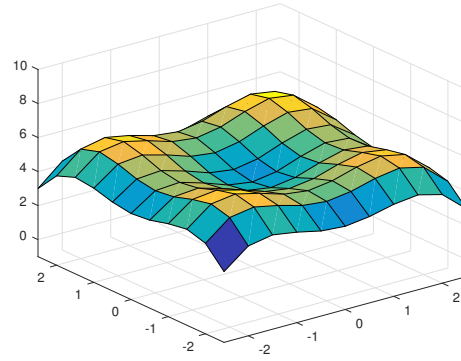
(b) Random Square Geometry Power Allocation

(c) Random Circumcircle Geometry

(d) Random Superposition Geometry

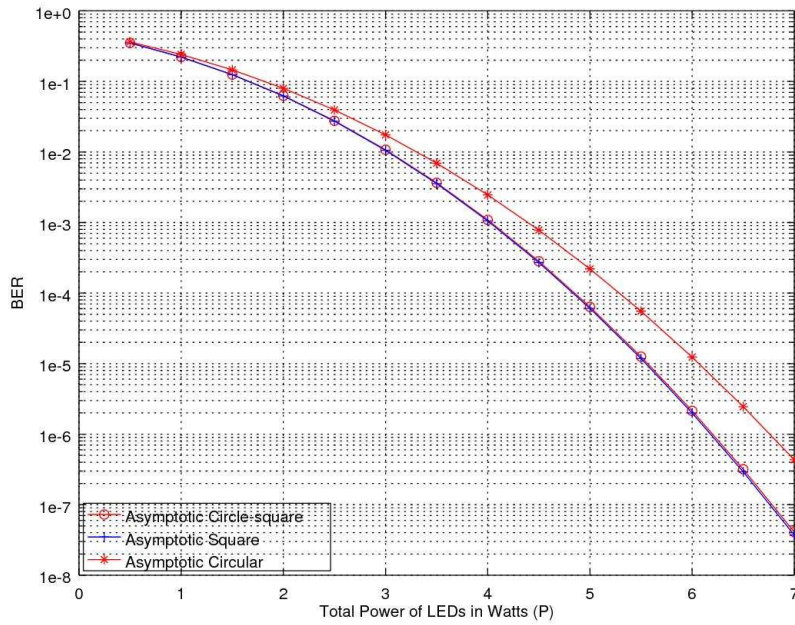Figure 5.2: Irradiance profile with power allocation
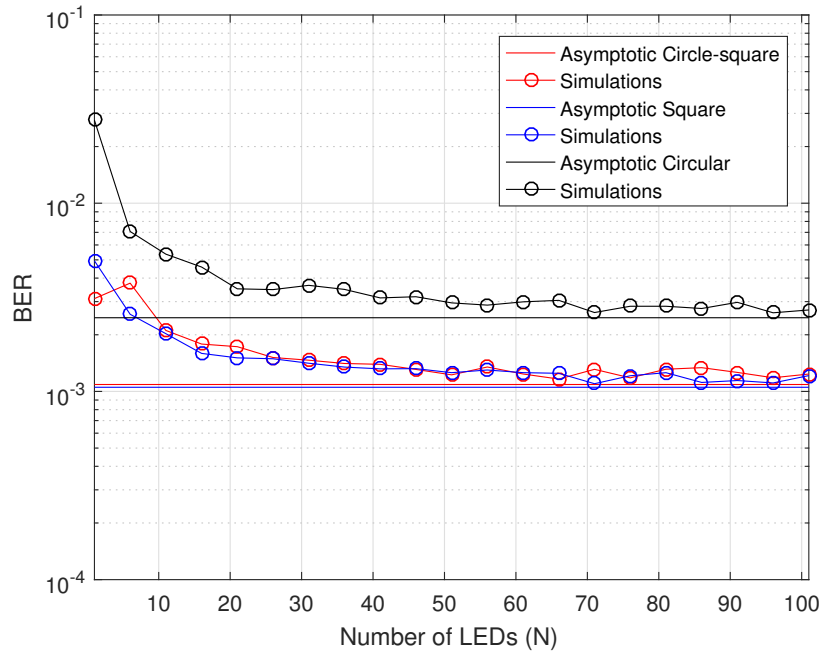
Figure 5.3: BER for various geometries

Figure 5.4: Simulated BER matches the theoretical asymptotic BER for large N.

BPPs. For the square BPP, simulation results are available in Fig. 5.3. As expected, the circle-square geometry mimics the square geometry, both in terms of the SNR profile as well as the BER.

Fig. 5.4 shows the simulated BER behavior for all geometries with increasing number of LEDs. It is obvious from the figure that after $N = 20$, the BER performance is close to the asymptotic BER. Also, the shape of the simulated BER curves for circular and square geometries is similar. Thus, the closed form BER expression for the asymptotic BER can be used to estimate the cost of the system in terms of the number of LEDs.

5.4 Appendix

5.4.1 Proof for the CDF of Circle-square BPP

The center of the circle is located at origin and not necessarily coincides with a point of the process. Observe that if a circle of radius r contains exactly $(n - 1)$ points and the nth point is located at the circumference, r is the distance to the nth neighbor of origin. The probability that a circle contains exactly n points is $\binom{N}{n} p^n (1 - p)^{N-n}$.

The complementary cumulative distribution function (CCDF) is the probability that there are less than n points in a circle is given by [28]

$$\bar{F}_{r_n}(r) = \sum_{k=0}^{n-1} \binom{N}{k} p^k (1 - p)^{N-k} \tag{5.9}$$

where $p = \frac{\mathcal{A}(\mathcal{B}(o,r) \cap W)}{\mathcal{A}(W)}$, and $\mathcal{A}(.)$ area of region, W is the region where points are distributed, $B(o, r)$ is ball of radius r with center origin.

Calculating p

$p = \frac{\mathcal{A}(B(o,r) \cap W)}{\mathcal{A}(W)}$
From Fig. 5.1,

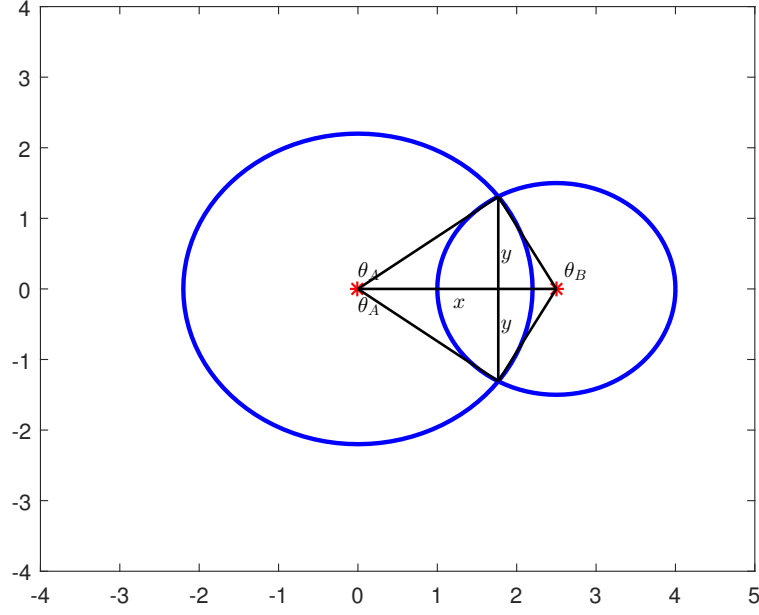$$\mathcal{A}(W) = \pi \left((L/2)^2 + 4k^2 \right) \tag{5.10}$$

Figure 5.5: Area of intersection of two circles.

where $k = \frac{\left(3 - 2\sqrt{2}\right)L}{2}$.

From Fig. 5.6,

$$\mathcal{A}\left(B\left(o, r\right) \cap W\right) = \begin{cases} \pi r^2 & 0 < r < L/2 \\ \pi \left(\frac{L}{2}\right)^2 + 4\left(\theta_A r^2 + \theta_B k^2 - dy\right) & L/2 < r < L/2 + 2k \\ \pi \left((L/2)^2 + 4k^2\right) & r > L/2 + 2k \end{cases} \quad (5.11)$$

where d is distance between the centers of the circles and

$$\theta_A = \cos^{-1}\left(\frac{x}{r}\right) \qquad \theta_B = \cos^{-1}\left(\frac{d - x}{k}\right) \qquad x = \frac{r^2 - k^2 + d^2}{2d} \qquad y = \sqrt{r^2 - x^2}$$

$$(5.12)$$

$$p = \begin{cases} \frac{r^2}{(L/2)^2 + 4k^2} & 0 < r < L/2 \\ \frac{\pi\left(\frac{L}{2}\right)^2 + 4\left(\theta_A r^2 + \theta_B k^2 - dy\right)}{\pi\left((L/2)^2 + 4k^2\right)} & L/2 < r < L/2 + 2k \\ 1 & r > L/2 + 2k \end{cases} \quad (5.13)$$
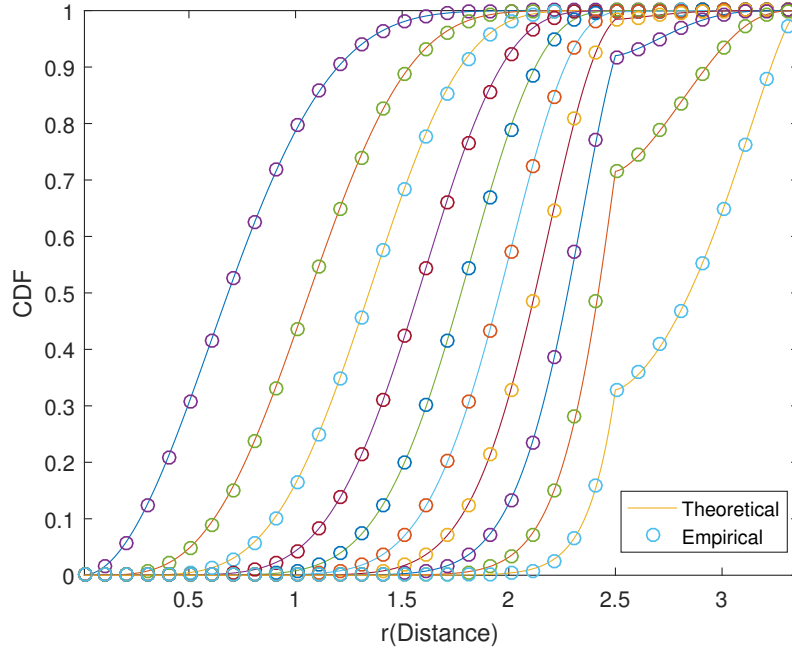
The pdf of the distance function of nth LED is then

39

Figure 5.6: CDF of nth nearest neighbor for BPP of N=10 in W.

$$f_{r_n}(r) = \frac{-d\bar{F}_{r_n}(r)}{dr} \tag{5.14}$$

$$= \frac{dp}{dr} \frac{(1-p)^{N-n} p^{n-1}}{\mathcal{B}(N-n+1,n)} \tag{5.15}$$

Calculation of $\frac{dp}{dr}$

$$\frac{dp}{dr} = \begin{cases} \frac{2r}{(L/2)^2+4k^2} & 0 < r < L/2 \\ \frac{4(\theta'_A r^2 + 2\theta_A r + \theta'_B k^2 - dy')}{\pi((L/2)^2+4k^2)} & L/2 < r < L/2 + 2k \\ 0 & r > L/2 + 2k \end{cases} \tag{5.16}$$

$$\theta'_A = \frac{(x-rx')}{r\sqrt{r^2-x^2}} \qquad \theta'_B = \frac{x'}{\sqrt{k^2-y^2}} \qquad x' = \frac{r}{d} \qquad y' = \frac{r-xx'}{\sqrt{r^2-x^2}} \tag{5.17}$$

Using (5.13) and (5.16) in (8.9), PDF is obtained.

■

5.4.2 Proof for Circle-square BPP

The expectation of the variable V_i has to be evaluated to derive the probability of error P_e. The PDF of the distance variable r_i is derived in the previous section.

$$\mathbb{E}_\Phi\left[r_i^\alpha\right] = \int_0^{\frac{L}{2}+2k} r^\alpha dF_{r_i}(r) \tag{5.18}$$

By Stieltjes integral,

$$\mathbb{E}_\Phi\left[r_i^\alpha\right] = r^\alpha F_{r_i}(r)\big|_0^{\frac{L}{2}+2k} - \alpha \int_0^{\frac{L}{2}+2k} r^{\alpha-1} F_{r_i}(r)dr$$

$$= \left(\frac{L}{2}+2k\right)^\alpha - \alpha \int_0^{\frac{L}{2}+2k} r^{\alpha-1} F_{r_i}(r)dr$$

Averaging V_i over the point process, we obtain

$$\mathbb{E}_\Phi\left[V_i\right] = \frac{1}{\sum_{j=1}^N \mathbb{E}_\Phi\left[r_j^\alpha\right]} \int_0^\infty \frac{r^\alpha dF_{r_i}(r)}{\left(\sqrt{r^2+h^2}\right)^{m+3}}$$

$$= \frac{1}{\sum_{j=1}^N \mathbb{E}_\Phi\left[r_j^\alpha\right]} \left[\frac{r^\alpha}{\left(\sqrt{r^2+h^2}\right)^{m+3}} F_{r_i}(r) \Bigg|_0^{\frac{L}{2}+2k} \right.$$

$$\left. - \int_0^{\frac{L}{2}+2k} \frac{r^{\alpha-1}\left(r^2\left(\alpha-m-3\right)+h^2\alpha\right)F_{r_i}(r)}{\left(\sqrt{r^2+h^2}\right)^{m+5}} dr \right]$$

$$= \frac{1}{\sum_{j=1}^N \mathbb{E}_\Phi\left[r_j^\alpha\right]} \left[\frac{\left(\frac{L}{2}+2k\right)^\alpha}{\left(\sqrt{\left(\frac{L}{2}+2k\right)^2+h^2}\right)^{m+3}} \right.$$

$$\left. - \int_0^{\frac{L}{2}+2k} \frac{r^{\alpha-1}\left(r^2\left(\alpha-m-3\right)+h^2\alpha\right)F_{r_i}(r)}{\left(\sqrt{r^2+h^2}\right)^{m+5}} dr \right].$$

Chapter 6

Optimum Power Allocation for Uniform Illuminance in Visible Light Communication

In existing VLC systems, uniform illumination is obtained by finding higher order partial derivatives of the received power at a point close to origin and equating to zero [1, 2]. This ensures uniformity only in the neighbourhood of origin. Similar approach has been used to obtain optimum spacing between LEDs in square array and optimum radii in case of circular arrays [3,4]. Local search algorithm is employed to find the optimum location of the LEDs [23]. The solution is obtained by iterative process and may not be optimum if the time bound is elapsed.

In chapter 4, we presented our earlier work, where light sources are modeled using stochastic geometry by locating them randomly in an indoor environment, generating average uniform illumination with appropriate power allocation. While a binomial point process (BPP) based stochastic model is a powerful tool for resource allocation for VLC, it is useful to consider power allocation for a VLC based on a single realization of a stochastic point process. Here, a Matern type II hard-core point process (HCPP) is desirable, since it accounts for minimum separation between any two LEDs for better coverage. This allows the realizations of the point process to be more uniformly distributed than BPP. The solution to this problem is presented in this chapter.

We have established that an appropriate power allocation to a random arrangement of the source LEDs in BPP results in uniform illuminance in an average sense. The optimal distribution of the power across the light sources for uniform illuminance for a single realisation of a point process is an important problem in a VLC. This is

addressed in this chapter.

6.1 Problem Definition

For uniform illumination, it is important that the mean $\overline{\Lambda}$ be large and the variance $\mathrm{var}(\Lambda)$ be small. Since the output of the photo-detector is an electrical signal which is affected by noise, it is important to consider the SNR Λ_j while computing the quality factor F_Λ. Since the SNR at the receiver is proportional to square of received power (or received power) in low transmit power regime (high transmit power), the power allocation for uniform illuminance also results in uniform SNR.

For the uniform illuminance in VLC system, the power received at any photo detector on the receiver plane should be same. Since the photo detectors can be located at any point in the plane, the variance of the received power is considered as a objective function to be minimized

$$\min_{P_{t_i}} \quad \mathbb{E}\left[\left(P_{r_j} - \mathbb{E}\left[P_{r_j}\right]\right)^2\right] \tag{6.1}$$

This can be formulated as an optimization problem.

6.2 Optimum Power Allocation

Lemma 6.2.1. The objective function in (6.1) is expressed in quadratic form as

$$\begin{aligned}
\min_{x} \quad & \frac{1}{2}\mathbf{x}^T \mathcal{P}\mathbf{x} \\
\text{subject to} \quad & \mathcal{G}\mathbf{x} \preceq \mathbf{0} \\
& \mathcal{A}\mathbf{x} = P
\end{aligned} \tag{6.2}$$

where $\mathcal{G} = \mathrm{diag}(-1, \cdots, -1)$, $\mathbf{x} = [P_{t_1}, \cdots, P_{t_N}]^T$, $\mathcal{A} = [1, \cdots, 1]$, the matrix $\mathcal{P}$ is given by

$$\mathcal{P} = \begin{bmatrix} \beta_{11} & \cdots & \beta_{1N} \\ \vdots & \ddots & \vdots \\ \beta_{N1} & \cdots & \beta_{NN} \end{bmatrix} \tag{6.3}$$

Table 6.1: Simulation parameters

Parameters	Symbol	Configuration
Room size	$L \times B \times D$	$5m \times 5m \times 3m$
Hieght of receiver plane	h_r	$0.85m$
LED semiangle	$\phi_{\frac{1}{2}}$	60°

and elements β_{uv} are

$$
\beta_{uv} = \begin{cases} \frac{2\sum_{p=1}^{K} H_{up}^2}{K} - \frac{2\left(\sum_{p=1}^{K} H_{up}\right)^2}{K^2}, & u = v \\ \frac{2\sum_{p=1}^{K} H_{up}H_{vp}}{K} - \frac{2\left(\sum_{p=1}^{K} H_{up}\right)\left(\sum_{p=1}^{K} H_{vp}\right)}{K^2}, & u \neq v \end{cases} \tag{6.4}
$$

Proof. See Appendix 6.4.1

The cost function in (6.2) is convex iff $\mathcal{P}$ is positive-definite [40]. Since the variance of received power $\mathbf{x}^T\mathcal{P}\mathbf{x} > 0 \quad \forall \quad \mathbf{x} \in \mathbb{R}_+^N$, $\mathcal{P}$ is positive-definite. Since the linear functions are both convex and concave, all the constraints are convex. Thus the optimization problem in (6.2) yields a quadratic and convex optimization problem. It can be numerically solved using quadratic programming (QP) through the solvers.qp command using CVXOPT solver in Python .

6.3   Results

All the physical parameters for the system have been obtained from [11] and Table 6.1.

The values of $\alpha = 1.1, 1.2, 3.1, 1.6$ of heuristic power allocation for Square, Circle Square, BPP and HCPP geometries respectively are obtained by golden section search algorithm. The variance and quality factor for different power allocation in different geometries have been tabulated in 6.2 and 6.3. It can be seen that the optimum solution obtained by solving (6.2) gives the minimum variance and better quality factor. The circle square geometry in [21] gives best quality factor, because of considering sub-optimal location of LEDs. All results indicate that more the LEDs are distributed, more uniformity can be achieved with optimum power allocation.

In Fig. 6.1 the SNR profiles of different geometries for equal and optimum power allocation schemes are plotted. Note that SNR profile of HCPP is for one realization of the point process. In Fig. 6.2 the optimal allocation of total transmit power $P = 2W$ across 16 source LEDs distributed according to HCPP is shown. It was observed that

Table 6.2: Variance of Received Power

Geometry	Equal Power	Heuristic[25]	Optimum
Square Array	6.4414e-15	6.5287e-16	6.3785e-16
Circle Square	3.0134e-15	1.1267e-15	8.0382e-16
BPP	2.5589e-14	5.4944e-15	2.7167e-15
HCPP (16 $LEDs$)	6.9160e-13	1.9802e-13	3.3046e-14
HCPP (13 $LEDs$)	4.4503e-13	1.5460e-13	3.3027e-14

Table 6.3: Quality factor

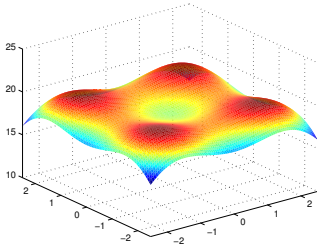| Geometry	Equal Power	Heuristic[25]	Optimum
Square Array	1.24	3.30	3.28
Circle Square	3.79	4.48	5.06
BPP	1.27	2.80	3.49
HCPP (16 $LEDs$)	1.16	1.92	4.26
HCPP (13 $LEDs$)	1.39	2.10	4.26
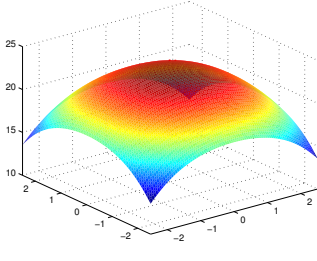
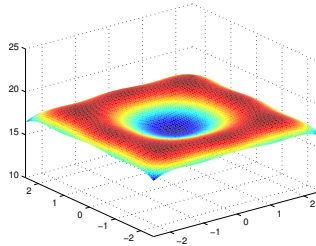
(a) Square array with equal power
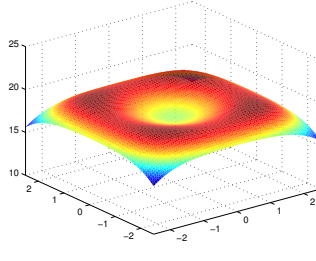
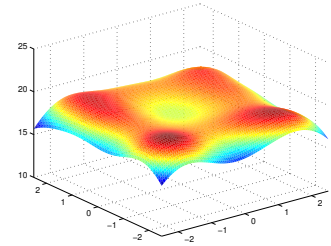(b) Circle square geometry with equal power
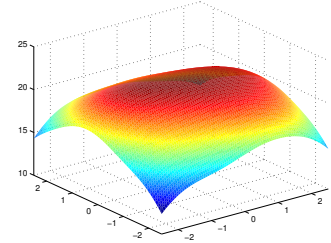
(c) HCPP with equal power

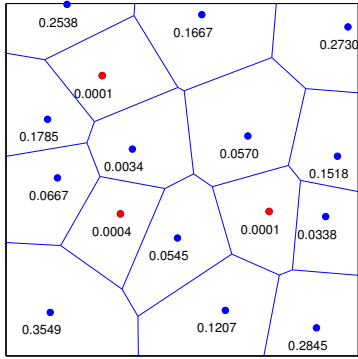(d) Square array with optimum power
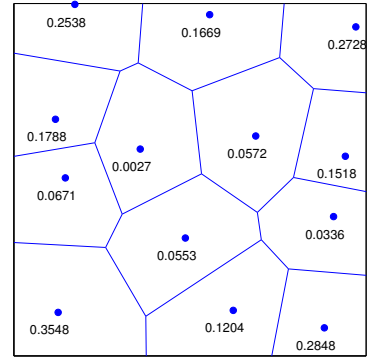
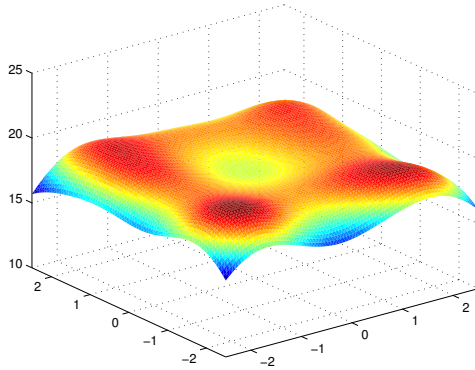(e) Circle square geometry with optimum power

(f) HCPP with optimum power

Figure 6.1: SNR profiles for different geometries.
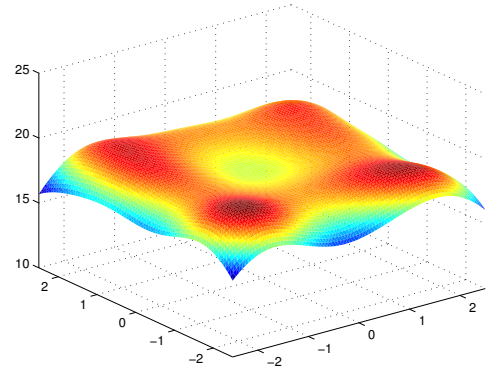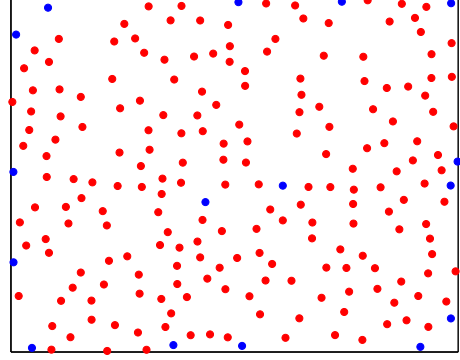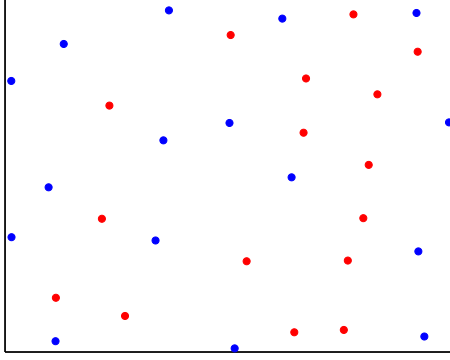
(a) HCPP with N=16 LEDs

(b) HCPP with N=13 LEDs

(c) SNR profile of 16 LED realization of HCPP

(d) SNR profile of 13 LED realization of HCPP

Figure 6.2: Optimal distribution of total transmit power across source LEDs and their SNR profiles.

(a) HCPP with intensity N=32 and threshold 0.0027

(b) HCPP with intensity N=200 and threshold 0.017
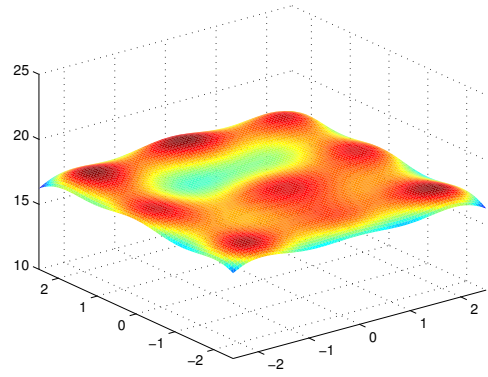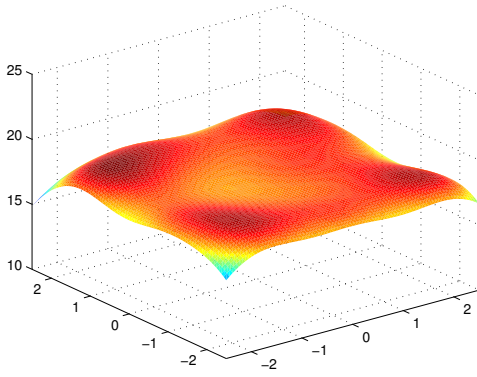
(c) SNR profile of the above realization resulting in quality factor $F_\Lambda = 6.29$

(d) SNR profile of the above realization resulting in quality factor $F_\Lambda = 11.35$

Figure 6.3: Optimal distribution of total transmit power across source LEDs and their SNR profiles.

3 source LEDs marked red in Fig. 6.2a have insignificant transmit power compared to others. Hence, these LEDs are taken out of geometry in Fig. 6.2b keeping others at the same location. The optimum power allocation for these remaining 13 LEDs obtained once again through solvers still preserves uniform illuminance. This can be seen from Table 6.2 and 6.3, the variance and the quality factor of the HCPP model realization with 13 source LEDs is close to the realization with 16 LEDs, thus reducing the cost of the system.

In Fig. 6.3 the source LEDs are distributed according to HCPP with intensity of 32 and 200. The LEDs are taken out of geometry in Fig. 6.3a and Fig. 6.3b, in case the transmitted power is less than threshold. It is observed from Fig. 6.2a, Fig. 6.3a and Fig. 6.3b that the uniformity and the quality factor are improved for the same

Figure 6.4: Performance of HCPP model with intensity N = 200.

Table 6.4: Quality factor

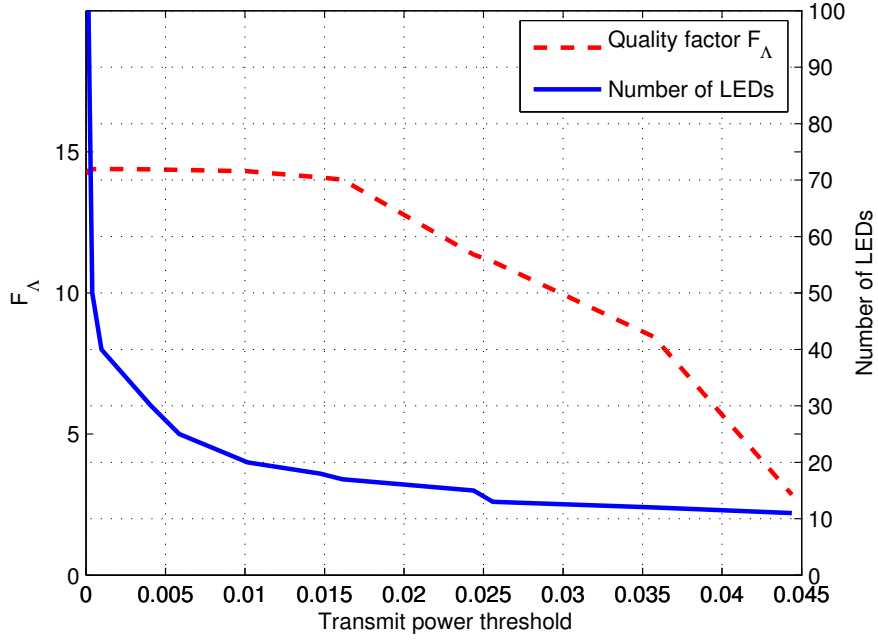| Intensity of HCPP	Transmit power threshold	Number of LEDs remaining for realization	Quality factor
16	0	16	4.26
32	2.7e-3	16	6.29
200	1.7e-2	16	11.34
	1.6e-2	17	14.02

number of LEDs. This improvement can be attributed to optimum location of LEDs.

In Fig. 6.4 the quality factor and number of source LEDs are plotted with respect to the transmit power threshold. It can be seen that the quality factor saturates as the number of source LEDs increases. For a ideal VLC system, the high quality factor should be achieved with the less number of source LEDs. Hence, there is a trade-off between the number of LEDs and the quality factor. For example, at threshold value of 0.016 the quality factor is 14.02 and close to the saturated value. The number of LEDs required for obtaining that quality factor is 17. Thus, the performance curves in Fig. 6.4 can be used to estimate the cost of the VLC system in terms of the number of LEDs.

6.4   Appendix

6.4.1   Formulation of optimization problem

Cost function

The first term in (6.1) is expressed in terms of transmit power as

$$
\begin{aligned}
\mathbb{E}\left[\left(P_{r_j}\right)^2\right] &= \mathbb{E}\left[\left(\sum_{i=1}^{N} H_{ij} P_{t_i}\right)^2\right] \qquad \text{(From (2.7))} \\
&= \mathbb{E}\left[\sum_{i=1}^{N} H_{ij}^2 P_{t_i}^2 + 2\sum_{i=1}^{N}\sum_{q=i+1}^{N} H_{ij} H_{qj} P_{t_i} P_{t_q}\right] \\
&= \frac{\sum_{j=1}^{K}\sum_{i=1}^{N} H_{ij}^2 P_{t_i}^2}{K} + \frac{\sum_{j=1}^{K} 2\sum_{i=1}^{N}\sum_{q=i+1}^{N} H_{ij} H_{qj} P_{t_i} P_{t_q}}{K} \\
&= \frac{\sum_{i=1}^{N} \mu_{ii} P_{t_i}^2 + 2\sum_{i=1}^{N}\sum_{q=i+1}^{N} \mu_{iq} P_{t_i} P_{t_q}}{K} \qquad (6.5) \\
&\text{where } \mu_{iq} = \sum_{j=1}^{K} H_{ij} H_{qj}.
\end{aligned}
$$

Similarly, the second term is expressed as

$$
\begin{aligned}
\left(\mathbb{E}\left[P_{r_j}\right]\right)^2 &= \left(\frac{\sum_{j=1}^{K} P_{r_j}}{K}\right)^2 \\
&= \left(\frac{\sum_{j=1}^{K}\sum_{i=1}^{N} H_{ij} P_{t_i}}{K}\right)^2
\end{aligned}
$$

$$= \left(\frac{\sum_{i=1}^{N} \gamma_i P_{t_i}}{K} \right)^2 \text{ where } \gamma_i = \sum_{j=1}^{K} H_{ij}$$

$$= \frac{\sum_{i=1}^{N} \gamma_i^2 P_{t_i}^2 + 2 \sum_{i=1}^{N} \sum_{p=i+1}^{N} \gamma_i \gamma_p P_{t_i} P_{t_p}}{K^2}. \tag{6.6}$$

Using (6.6) and (6.5) in (6.1), variance is represented in matrix form as

$$
\begin{aligned}
\text{var}\left(P_{r_j}\right) &= \frac{\sum_{i=1}^{N} \mu_{ii} P_{t_i}^2 + 2 \sum_{i=1}^{N} \sum_{q=i+1}^{N} \mu_{iq} P_{t_i} P_{t_q}}{K} \\
&\quad - \frac{\sum_{i=1}^{N} \gamma_i^2 P_{t_i}^2 + 2 \sum_{i=1}^{N} \sum_{p=i+1}^{N} \gamma_i \gamma_p P_{t_i} P_{t_p}}{K^2} \\
&= \sum_{i=1}^{N} \frac{\mu_{ii}}{K} - \frac{\gamma_i^2}{K^2} P_{t_i}^2 + 2 \sum_{i=1}^{N} \sum_{q=i+1}^{N} \frac{\mu_{iq}}{K} - \frac{\gamma_i \gamma_p}{K^2} P_{t_i} P_{t_q} \\
&= \frac{1}{2} \sum_{i=1}^{N} \left(\frac{2 \sum_{j=1}^{K} H_{ij}^2}{K} - \frac{2 \left(\sum_{j=1}^{K} H_{ij} \right)^2}{K^2} \right) P_{t_i}^2 \\
&\quad + 2 \sum_{u=1}^{N} \sum_{v=i+1}^{N} \left(\frac{2 \sum_{j=1}^{K} H_{uj} H_{vj}}{K} - \frac{2 \left(\sum_{j=1}^{K} H_{uj} \right) \left(\sum_{j=1}^{K} H_{vj} \right)}{K^2} \right) P_{t_u} P_{t_v} \\
&= \frac{1}{2} \left[P_{t_1}, \cdots, P_{t_N} \right] \begin{bmatrix} \beta_{11} & \cdots & \beta_{1N} \\ \vdots & \ddots & \vdots \\ \beta_{N1} & \cdots & \beta_{NN} \end{bmatrix} \begin{bmatrix} P_{t_1} \\ \vdots \\ P_{t_N} \end{bmatrix} \\
&= \frac{1}{2} \mathbf{x}^T \mathcal{P} \mathbf{x}. \tag{6.7}
\end{aligned}
$$

Constraints

1. The total power of the LEDs is P watts, which is distributed across the source LEDs.

$$\sum_{i=1}^{N} P_{t_i} = P$$

$$\Rightarrow \mathcal{A}\mathbf{x} = P$$

where $\mathcal{A} = [1, \cdots, 1]$.

2. The power of each source LED is always non-negative.

$$-P_{t_i} \leq 0 \quad \forall \quad i \in 1, \cdots, N$$

which can be expressed in matrix form as

$$\Rightarrow \mathcal{G}\mathbf{x} \preceq \mathbf{0}$$

where $\mathcal{G} = \text{diag}(-1, \cdots, -1)$.

Chapter 7

Conclusion

In this dissertation, it was shown that distributed LED sources that do not follow a locational pattern can be modeled using a BPP with appropriate power allocation, to achieve uniform illumination. This makes it extremely useful in practical applications like visible light communication where the source geometry is likely to be random. Though sub-optimal, the proposed heuristic for power allocation is much simpler, resulting in reduced computational cost, when compared to existing optimal power allocation schemes.

An approximate closed form expression for the asymptotic BER has been obtained for a square and a circular BPP. This expression was used to assess system performance with respect to the source power as well as the number of LEDs. This allows for estimating the cost of the system in terms of these two parameters which has significant application in the design of practical VLC systems.

The optimization of power allocation to source LEDs for uniform illumination in VLC is addressed in this thesis. The problem was formulated as a quadratic optimization problem and resolved numerically using CVXOPT solver. Numerical results demonstrate that the uniform illumination can be achieved even when all light sources are distributed randomly, in contrast with the existing fixed geometries like circular and square arrays. It was observed that HCPP model can preserve uniformity

with less number of LEDs compared to other geometries, thus reducing the cost of the system.

Thus a VLC system can be designed using the estimated number of LEDs, with intuitive LED arrangement and the power requirement for an appropriate BER, and inclusion of optimum power allocation ensuring uniform SNR.

7.1 Future Research

- As the immediate extension to the work, the performance of VLC in terms of BER when HCPP is used for modeling the LED arrangement would be a challenging problem. The distribution of nearest neighbor for HCPP is existing in the literature. In order to solve this, we have to find the distribution of nth LED from the origin.

- People have considered localization of LEDs for uniform illuminance [1–4, 12]. We have looked at power allocation of LEDs irrespective of their location. It would be interesting to optimize the location and power allocation jointly.

- There are few practical challenges like Non-line of sight (NLOS), modulation techniques, channel equalization, that are not considered in this dissertation. Building a VLC and experimental results helps in better understanding of these challenges.

Publications from the Thesis

Published

1. G. V. S. S. Praneeth Varma, Rayapati Sushma, Vandana Sharma, Abhinav Kumar, and G. V. V. Sharma, "Power Allocation for Uniform Illumination with Stochastic LED Arrays," *Opt. Express*, vol. 25, no. 8, pp. 8659–8669, Apr. 2017.

2. G. V. S. S. Praneeth Varma, "Optimum Power Allocation for Uniform Illuminance in Visible Light Communication," in Proc. *National Conference on Communicaitons (NCC)*, Feb 2018.

3. G. V. S. S. Praneeth Varma, Abhinav Kumar and G. V. V. Sharma, "Resource Allocation for Visible Light Communication using Stochastic Geometry," in Proc. *IEEE CSNDSP*, July 2018.

4. G. V. S. S. Praneeth Varma, "Optimum Power Allocation for Uniform Illuminance in Visible Light Communication," *Opt. Express*, vol. 26, no. 7, pp. 8679–8689, Apr. 2018.

Chapter 8

Mathematical Contributions of the Thesis

Some of the interesting mathematical results obtained during the course of this thesis are presented here in this chapter. These theorems are relevant to stochastic geometry and are likely to be useful for research in this field of applied mathematics.

8.1 Distance distributions of square BPP

Theorem 8.1.1. The cumulative distribution function (CDF) of the distance to the nth neighbor from any location (x,y) is

$$F_{r_n}(r) = \frac{\pi r^2 - \sum_{i=1}^{4} U(r - d_{E_i}) Z_1(r, d_{E_i}) + \sum_{i=1}^{4} U(r - d_{V_i}) Z_2(r, \beta_i, \gamma_i, d_{V_i})}{L^2} \quad (8.1)$$

where

$$Z_1(z, a) = \frac{z^2}{2} \left(cos^{-1} \left(\frac{a}{z} \right) - \sin \left(2cos^{-1} \left(\frac{a}{z} \right) \right) \right) \quad (8.2)$$

$$Z_2(z, \beta_i, \gamma_i, d_{V_i}) = \frac{1}{2} \left(z^2 \left(\theta - \sin(\theta) \right) + \beta_i \gamma_i \right) \quad (8.3)$$

and $\theta = cos^{-1} \left(\frac{d_{V_i}^2 + r^2 - \beta_i^2}{2 d_{V_i} r} \right) + cos^{-1} \left(\frac{d_{V_i}^2 + r^2 - \gamma_i^2}{2 d_{V_i} r} \right)$

d_{E_i} is the distance of the edges from point (x, y), d_{V_i} is the distance of the vertices from point (x, y) and L is the side of the Square region W where points are distributed.

Proof. The center of the circle a i.e. (x,y) is located at random and not necessarily coincides with a point of the process. Observe that if a circle of radius r contains

Table 8.1: Distance parameters

	d_{E_i}	d_{V_i}	β_i	γ_i
i=1	$\frac{L}{2}-y$	$\sqrt{(\frac{L}{2}-x)^2+(\frac{L}{2}-y)^2}$	$\sqrt{r^2-\left(\frac{L}{2}-x\right)^2}-\left(\frac{L}{2}-y\right)$	$\sqrt{r^2-\left(\frac{L}{2}-y\right)^2}-\left(\frac{L}{2}-x\right)$
i=2	$\frac{L}{2}-x$	$\sqrt{(\frac{L}{2}+x)^2+(\frac{L}{2}-y)^2}$	$\sqrt{r^2-\left(\frac{L}{2}+x\right)^2}-\left(\frac{L}{2}-y\right)$	$\sqrt{r^2-\left(\frac{L}{2}-y\right)^2}-\left(\frac{L}{2}+x\right)$
i=3	$\frac{L}{2}+x$	$\sqrt{(\frac{L}{2}-x)^2+(\frac{L}{2}+y)^2}$	$\sqrt{r^2-\left(\frac{L}{2}-x\right)^2}-\left(\frac{L}{2}+y\right)$	$\sqrt{r^2-\left(\frac{L}{2}+y\right)^2}-\left(\frac{L}{2}-x\right)$
1=4	$\frac{L}{2}+y$	$\sqrt{(\frac{L}{2}+x)^2+(\frac{L}{2}+y)^2}$	$\sqrt{r^2-\left(\frac{L}{2}+x\right)^2}-\left(\frac{L}{2}+y\right)$	$\sqrt{r^2-\left(\frac{L}{2}+y\right)^2}-\left(\frac{L}{2}+x\right)$

exactly $(n-1)$ points and the nth point is located at the circumference, r is the distance to the nth neighbor of a. The probability that a circle contains exactly n points is $\binom{N}{n}p^n (1-p)^{N-n}$

The complementary cumulative distribution function (CCDF) is the probability that there are less than n points in a circle is given by [28]

$$\bar{F}_{r_n}(r) = \sum_{k=0}^{n-1} \binom{N}{k} p^k (1-p)^{N-k} \tag{8.4}$$

where $p = \frac{g(r)}{\mathcal{A}(W)} = p = \frac{\mathcal{A}(\mathcal{B}(o,r)\cap W)}{\mathcal{A}(W)}$, and $\mathcal{A}(.)$ area of region, W is the region where points are distributed, $\mathcal{B}(a,r)$ is ball of radius r with center a.

8.1.1   Calculating g(r)

$$g(r) = \mathcal{A}(\mathcal{B}(o,r) \cap W) \tag{8.5}$$

$$A = A1 - A2 - A3 + A4 \tag{8.6}$$

Finding the distribution from any random point is same as finding the distribution of its projection in the first quadrant. Also, the distribution from random point (x,y) is same as from (y,x) because of symmetry.

WLOG, $y > x$, the general expression for $g(r)$ is expressed as

$$\pi r^2 - \sum_{i=1}^{4} U(r-d_{E_i})Z_1(r,d_{E_i}) + \sum_{i=1}^{4} U(r-d_{V_i})Z_2(r,\beta_i,\gamma_i,d_{V_i}) \tag{8.7}$$

The pdf of the distance function of nth LED from (x,y) is then

$$f_{r_n}(r) = \frac{-d\bar{F}_{r_n}(r)}{dr} \tag{8.8}$$

56

$$g(r) = B(0,r) \cap A$$
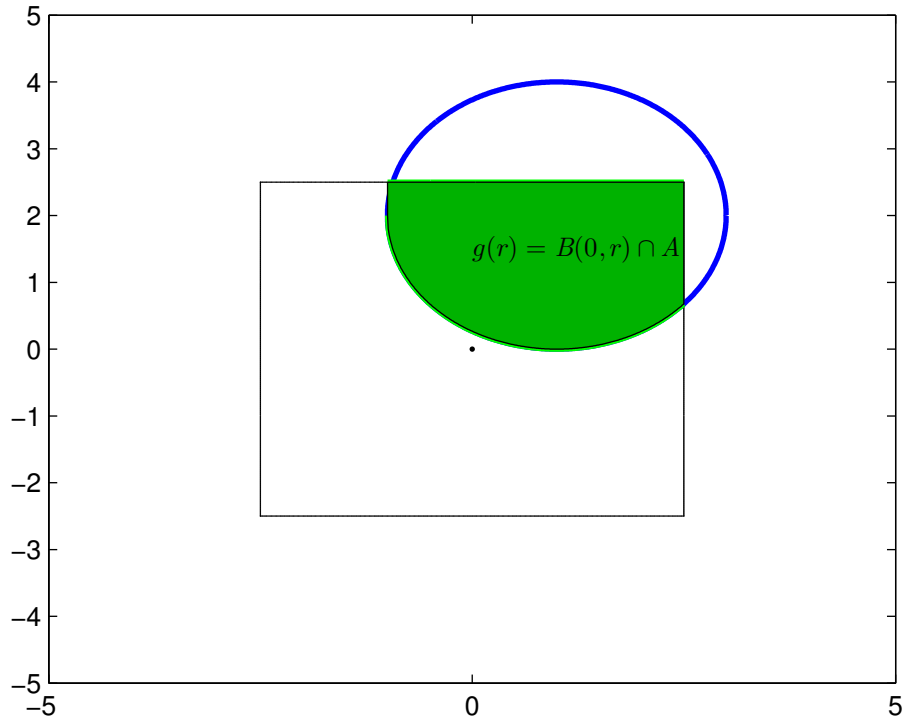
$$= \frac{dp}{dr} \frac{(1-p)^{N-n} p^{n-1}}{\mathcal{B}(N-n+1,n)} \tag{8.9}$$

where $\frac{dp}{dr} = \frac{g'(r)}{\mathcal{A}(W)}$

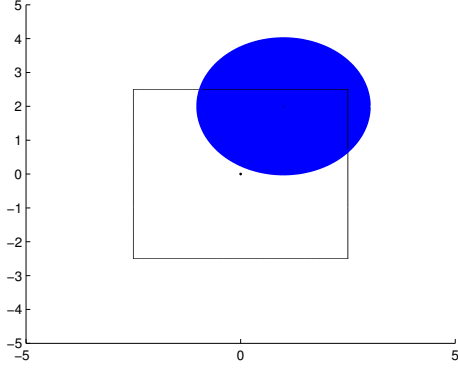## 8.2 Approximations in stochastic geometry

A commonly encountered integral in the coverage analysis using stochastic geometry based approach, as in [41] [42], is

$$\int_0^\infty e^{-Vt - Ut^{\frac{\alpha}{2}}} t^{\frac{n}{2}} \, dt. \tag{8.10}$$
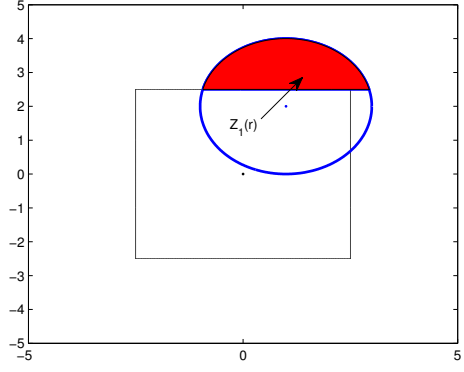
For approximating (8.10), we present the following theorem.

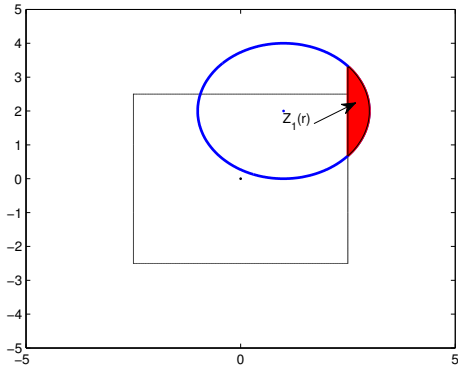**Theorem 8.2.1.** For $\alpha > 2$, $U > 0$, and $V > 0$,

$$\int_0^\infty e^{-Vt - Ut^{\frac{\alpha}{2}}} t^{\frac{n}{2}} \, dt \approx \frac{1}{V^{\frac{n+2}{2}}} \left[\gamma \left(n/2 + 1, \frac{V}{U^{2/\alpha}} x_1 \right) \right.$$
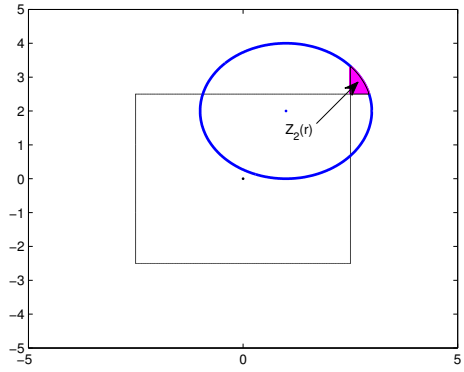
(a) Area of circle (A1)

(b) Area of non-overlapping segment 1: Z_1 (A2)

(c) Area of non-overlapping segment 2: Z_1 (A3)

(d) Area of non-overlapping segment removed twice: Z_2 (A4)

$$+ c \left\{ \gamma \left(n/2 + 1, \frac{V}{U^{2/\alpha}} x_2 \right) - \gamma \left(n/2 + 1, \frac{V}{U^{2/\alpha}} x_1 \right) \right\}$$
$$+ \frac{U^{2/\alpha}}{V} m \left\{ \gamma \left(n/2 + 2, \frac{V}{U^{2/\alpha}} x_2 \right) - \gamma \left(n/2 + 2, \frac{V}{U^{2/\alpha}} x_1 \right) \right\} \Bigg] , \quad (8.11)$$

where, $m = -\frac{\alpha}{2} \left(1 - \frac{2}{\alpha} \right)^{1 - \frac{2}{\alpha}} e^{-\left(1 - \frac{2}{\alpha} \right)}$, $c = \frac{\alpha}{2} e^{-(1 - \frac{2}{\alpha})}$, $x_1 = \frac{1-c}{m}$, $x_2 = \frac{-c}{m}$, and $\gamma \left(\cdot, \cdot \right)$ is the lower incomplete gamma function [39, 8.350].

Proof. The expression in (8.11) can be simplified to

$$\int_0^\infty e^{-Ut^{\alpha/2}} e^{-Vt} t^{\frac{n}{2}} dt = \frac{1}{U^{\frac{n+2}{\alpha}}} \int_0^\infty e^{-y^{\frac{\alpha}{2}}} e^{-\frac{V}{U^{2/\alpha}} y} y^{n/2} dy . \quad (8.12)$$

It is difficult to obtain an exact closed form solution for (8.12) for arbitrary α. From Fig. 8.2, it can be seen that $f(x) = e^{-x^{\alpha/2}}$ is monotonically decreasing w.r.t. x, $f(x) \in (0, 1] \, \forall x \geq 0$, and has a single point of inflection. Hence, for $f(x) = e^{-x^{\alpha/2}}$ a

58
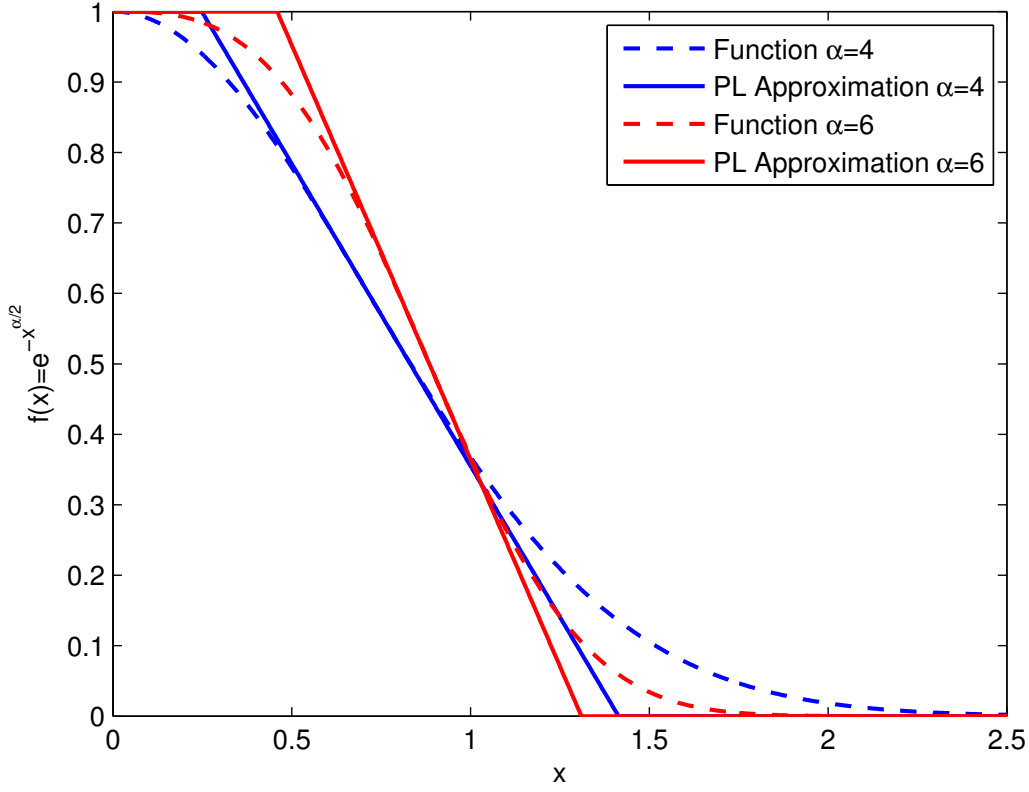
Figure 8.2: Piece-wise linear approximation

piece-wise linear approximation (PLA) is given by

$$
e^{-x^{\alpha/2}} \approx
\begin{cases}
1 & x \leq x_1\,, \\
mx + c & x_1 < x < x_2\,, \\
0 & x_2 \leq x\,,
\end{cases}
\tag{8.13}
$$

where, m, x_1, x_2, and c are unknown constants. To obtain m, we calculate the point of inflection of $f(x)$ denoted by x_0 as follows,

$$
\left. \frac{d^2(e^{-x^{\alpha/2}})}{dx^2} \right|_{x=x_0} = 0 \Rightarrow x_0 = \left(1 - \frac{2}{\alpha}\right)^{\frac{2}{\alpha}}.
\tag{8.14}
$$

Using (8.14), the slope at x_0, i.e., m is given by

$$
m = \left[\frac{d\left(e^{-x^{\frac{\alpha}{2}}}\right)}{dx} \right]_{x=x_0} = -\frac{\alpha}{2} \left(1 - \frac{2}{\alpha}\right)^{1-\frac{2}{\alpha}} e^{-\left(1-\frac{2}{\alpha}\right)}.
\tag{8.15}
$$

From (8.13), we have

$$
\begin{aligned}
1 &= mx_1 + c\,, \\
0 &= mx_2 + c\,, \\
e^{-x_0^{\alpha/2}} &= mx_0 + c\,,
\end{aligned}
\tag{8.16}
$$

for x equal to x_1, x_2, and x_0, respectively. The three linear equations in (8.16) can be jointly solved to obtain x_1, x_2, and c as given in (8.11).

Substituting the approximation (8.13) in (8.12), we get

$$
\frac{1}{U^{\frac{n+2}{\alpha}}} \left[\int_0^{x_1} y^{n/2} e^{-\frac{V}{U^{2/\alpha}}y} dy + \int_{x_1}^{x_2} (my+c) y^{n/2} e^{-\frac{V}{U^{2/\alpha}}y} \right] dy\,,
$$

which with transformation of variable results in

$$
\frac{1}{V^{\frac{n+2}{2}}} \left[\int_0^{\frac{V}{U^{2/\alpha}}x_1} x^{n/2} e^{-x} dx + c \int_{\frac{V}{U^{2/\alpha}}x_1}^{\frac{V}{U^{2/\alpha}}x_2} x^{n/2} e^{-x} dx + \frac{U^{2/\alpha}}{V} m \int_{\frac{V}{U^{2/\alpha}}x_1}^{\frac{V}{U^{2/\alpha}}x_2} x^{n/2+1} e^{-x} dx \right],
$$

and using definition of lower incomplete gamma function [39, 8.350] results in (8.11). This completes the proof of Theorem 8.2.1. ∎

This result has been applied in the area of heterogeneous networks using stochastic geometry techniques. We derive closed-form approximations of coverage probability and average rate in a downlink K-tier heterogeneous network in the presence of Nakagami-m fading and noise [43]. This approach is very simple with reduced time-complexity and provides accurate results.

References

[1] N. Wittels and M. A. Gennert, "Optimal Lighting Design to Maximize Illumina-
tion uniformity," *Proc. SPIE 2348, Imaging and Illumination for Metrology and
Inspection*, vol. 46, Oct. 1994.

[2] M. A. Gennert, N. Wittels, and G. L. Leatherman, "Uniform Frontal Illumina-
tion of Planar Surfaces: Where to Place the Lamps," *Opt. Eng.*, vol. 32, no. 6,
pp. 1261–1271, Nov. 2005.

[3] I. Moreno, "Design of led spherical lamps for uniform far-field illumination,"
Proc. SPIE 6046, Fifth Symposium Optics in Industry, vol. 6046, Feb. 2006.

[4] I. Moreno, M. Avendaño-Alejo, and R. I. Tzonchev, "Designing Light-emitting
Diode Arrays for Uniform Near-field Irradiance," *Appl. Opt.*, vol. 45, no. 10, pp.
2265–2272, 2006.

[5] Y. Liu, Y. Peng, Y. Liu, and K. Long;, "Optimization of receiving power dis-
tribution using genetic algorithm for visible light communication," *Proc. SPIE :
Optical Fiber Sensors and Applications*, vol. 9679, Oct. 2015.

[6] J. Ding, Z. Huang, and Y. Ji, "Evolutionary algorithm based power coverage
optimization for visible light communications," *IEEE Commun. Lett.*, vol. 16,
no. 4, Apr. 2012.

[7] S. Pal, "Optimization of led array for uniform illumination over a target plane
by evolutionary programming," *Appl. Opt.*, vol. 54, no. 27, pp. 8221–8227, 2015.

[8] H. Guo-yong, C. Chang-ying, and C. Zhen-qiang, "Free-space Optical Commu-
nication Using Visible Light," *Journal of Zhejiang University Science A.*, vol. 8,
no. 2, pp. 186–191, Feb 2007.

[9] J. Kovác, J. Jakabovic, and M. Kytka, "Advanced light emitting devices for optoelectronic applications," *Proc. SPIE , Photonics, Devices, and Systems IV*, vol. 7138, Nov. 2008.

[10] J. Kahn and J. Barry, "Wireless infrared communications," *Proc. IEEE*, vol. 85, no. 2, pp. 265–298, 1997.

[11] T. Komine and M. Nakagawa, "Fundamental analysis for visible-light communication system using led lights," *IEEE Trans. Consum. Electron.*, vol. 50, no. 1, pp. 100–107, Feb 2004.

[12] I. Moreno, "Configuration of led arrays for uniform illumination," *Proc. SPIE 5th Iberoamerican Meeting on Optics and 8th Latin American Meeting on Optics, Lasers, and Their Applications*, vol. 5622, pp. 713–718, Oct. 2004.

[13] Z. Qin, K. Wang, F. Chen, X. Luo, and S. Liu, "Analysis of Condition for Uniform Lighting Generated by Array of Light Emitting Diodes with Large View Angle," *Opt. Express*, vol. 18, no. 16, pp. 17 460–17 476, 2010.

[14] A. J. W. Whang, Y. Y. Chen, and Y. T. Teng, "Designing Uniform Illumination Systems by Surface-tailored Lens and Configurations of LED Arrays," *J. Disp. Technol.*, vol. 5, no. 3, pp. 94–103, Mar. 2009.

[15] K. Wang, D. Wu, Z. Qin, F. Chen, X. Luo, and S. Liu, "New Reversing Design Method for LED Uniform Illumination," *Opt. Express*, vol. 19, no. S4, pp. A830–A840, 2011.

[16] Y. Tanaka, T. Komine, S. Haruyama, and M. Nakagawa, "Indoor visible light transmission system utilizing white led lights," *IEICE Trans. on Communications*, vol. E86-B, no. 8, pp. 2440–2454, 2003.

[17] Y. Tanaka, S. Haruyama, and M. Nakagawa, "Wireless optical transmission with the white colored led for the wireless home link," *in Proc IEEE PIMRC*, pp. 1325–1329, 2000.

[18] T. Komine, Y. Tanaka, and S. H. andand M. Nakagawa, "Basic study on visible-light communication using light emitting diode illumination," *in Proc International Symposium on Microwave and Optical Technology*, pp. 45–48, 2001.

[19] H.-C. Chen, C.-J. Liou, and S.-. Siaoa, "Illumination distribution and signal transmission for indoor visible light communication with different light-emitting diode arrays and pre-equality circuits," *Opt. Eng.*, vol. 54, no. 11, 2015.

[20] T. Komine and M. Nakagawa, "Integrated system of white led visible-light communication and power-line communication," *IEEE Trans. Consum. Electron.*, vol. 49, no. 1, pp. 71–79, 2003.

[21] Z. Wang, C. Yu, W.-D. Zhong, J. Chen, and W. Chen, "Performance of a novel led lamp arrangement to reduce snr fluctuation for multi-user visible light communication systems," *Opt. Express*, vol. 20, no. 4, pp. 4564–4573, 2012.

[22] H. Zheng, J. Chen, C. Yu, and M. Gurusamy, "Inverse design of led arrangement for visible light communication systems," *Opt. Commun.*, vol. 382, pp. 615–623, Jan. 2017.

[23] P. Lei, Q. Wang, and H. Zou, "Designing led array for uniform illumination based on local search algorithm," *J. Europ. Opt. Soc. Rap. Public.*, vol. 9, no. 22, pp. 140 141–140 146, 2014.

[24] I. Neokosmidis, T. Kamalakis, J. Walewski, B. Inan, and T. Sphicopoulos, "Impact of nonlinear led transfer function on discrete multitone modulation: analytical approach," *J. Lightwave Technology*, vol. 27, no. 22, pp. 4970–4978, 2009.

[25] G. V. S. S. P. Varma, R. Sushma, V. Sharma, A. Kumar, and G. V. V. Sharma, "Power Allocation for Uniform Illumination with Stochastic LED Arrays," *Opt. Express*, vol. 25, no. 8, pp. 8659–8669, 2017.

[26] Y. Chen, C. W. Sung, S.-W. Ho, and W. S. Wong, "Ber analysis for interfering visible light communication systems," in *Proc. IEEE CSNDSP*, 2016.

[27] M. Haenggi, "Mean interference in hard-core wireless networks," *IEEE Commun. Lett.*, vol. 15, no. 8, pp. 792–794, 2011.

[28] S. Srinivasa and M. Haenggi, "Distance Distributions in Finite Uniformly Random Networks: Theory and Applications," *IEEE Trans. Veh. Technol.*, vol. 59, no. 2, pp. 940–949, Feb. 2010.

[29] W. H. Press, S. A. Teukolsky, W. T. Vetterling, and B. P. Flannery, *Numerical Recipes: The Art of Scientific Computing.* Cambridge University Press, 2007.

[30] A. Anusree and R. K. Jeyachitra, "Performance analysis of a mimo vlc (visible light communication) using different equalizers," in *Proc. IEEE WiSPNET*, 2016, pp. 43–46.

[31] R. Bai, R. Jang, J. Tan, and J. Quan, "Performance comparison of vlc mimo techniques considering indoor illuminance with inclined leds," in *Proc IEEE WiSEE*, 2016, pp. 105–110.

[32] P. F. Mmbaga, J. Thompson, and H. Haas, "Performance analysis of indoor diffuse vlc mimo channels using angular diversity detectors," *J. Lightwave Technol.*, vol. 34, no. 4, pp. 1254–1266, Feb 2016.

[33] L. Zeng, D. O'Brien, H. Le-Minh, K. Lee, D. Jung, and Y. Oh, "Improvement of date rate by using equalization in an indoor visible light communication system," in *Proc. IEEE CSCC*, 2008.

[34] H. Haas, L. Yin, Y. Wang, and C. Chen, "What is lifi?" *J. Lightwave Technology*, vol. 34, no. 6, pp. 1533–544, 2016.

[35] B. Sklar, *Digital Communications Fundamentals and Applications*, 2nd ed. Prentice Hall, 2001.

[36] S. G. Krantz, *Handbook of Complex Variables.* Birkhäuser, 1999.

[37] A. Stuart and K. Ord, *Kendall's Advanced Theory of Statistics Volume 1*, 6th ed., 1998.

[38] "Approximations for Mean and Variance of a Ratio of Random Variables," http://www.stat.cmu.edu/ hseltman/files/ratio.pdf.

[39] I. S. Gradshteyn and I. Ryzhik, *Table of Integrals, Series, and Products*, 7th ed. Elsevier/Academic Press, 2007.

[40] S.Boyd and L.Vandenberghe, *Convex Optimization.* Cambridge University Press, 2004.

[41] H. Dhillon, R. Ganti, F. Baccelli, and J. G. Andrews, "Modeling and analysis of k-tier downlink heterogeneous cellular networks," *IEEE J. Sel. Areas Commun.*, vol. 30, no. 3, pp. 550–560, April 2012.

[42] H. S. Dhillon, M. Kountouris, and J. G. Andrews, "Downlink mimo hetnets: Modeling,ordering results and performance analysis," *IEEE Trans. Wireless Commun.*, vol. 12, no. 10, pp. 5208–5222, October 2013.

[43] G. V. S. S. P. Varma, G. V. V. Sharma, and A. Kumar, "Closed-form approximations for coverage and rate in a multi-tier heterogeneous network in nakagami-m fading," *in Proc. NCC*, 2018.